Article:
Ji, W., Hong, F., Li, K. et al. (2025) Optimal dispatch of storage-assisted thermal power considering renewable uncertainties. Applied Thermal Engineering, 278 (Part C). 127276. ISSN: 1359-4311

https://doi.org/10.1016/j.applthermaleng.2025.127276

Optimal dispatch of storage-assisted thermal power considering renewable uncertainties

Weiming Ji[1,2,3], Feng Hong[1,2*], Kang Li[3], Lu Liang[1,2], Junhong Hao[1,4], Fang Fang[1,2], Jizhen Liu[1]

1. State Key Laboratory of Alternate Electrical Power System with Renewable Energy Sources (NCEPU), Beijing, 102206, China. 2. School of Control and Computer Engineering, North China Electric Power University, Beijing, 102206, China. 3. School of Electronic and Electrical Engineering, University of Leeds, Leeds LS2 9JT, UK. 4. School of Energy Power and Mechanical Engineering, North China Electric Power University, 102206 Beijing, China.

Abstract

Energy storage systems have emerged as critical components in modern power systems, addressing the challenges of frequency regulation stability and renewable integration. Coal-fired thermal power plants have provided grid stability but now confront increasing demands for deep peak shaving services. However, energy storage systems are exposed to relatively low energy support duration while thermal power units confront slow power changing rate. This paper proposes a coordinated control strategy and a robust optimization model for storage-assisted thermal power units, addressing short-term fluctuations and long-term uncertainties imposed on thermal power units across multiple timescales. The Column-and-Constraint Generation approach is employed to improve computational efficiency, achieving convergence within three iterations for the optimal solution. Simulation results confirm that the proposed uncertainty set effectively adapts to increasing data dimensions, addressing over-conservatism in traditional models subject to multi-timescale uncertainties. By leveraging the rapid response capability of energy storage and the steady output of thermal power units, the model improves grid support and alleviates operational stress on thermal units.The results also reveal that three different energy storage systems configurations result in cost reductions of 23.50%, 41.78%, and 38.63%, respectively, while demonstrating a substantial improvement in the system's resilience in response to short- and long-term challenges.

Keywords: Thermal power unit, energy storage system, multi-timescale, renewable energy uncertainties, column and constrain generation

Nomenclature

Abbreviations

ESS	Energy Storage System.
PV	Photovoltaic.
SOC	State of Charge.
STC	Standard Test Condition.
TPU	Thermal Power Unit.

*Corresponding author.
Email address: hongf@ncepu.edu.cn (Feng Hong[1,2])

WT Wind Turbine.

Symbols

α_{emi} The cost associated with emissions per unit of power.

α_{fc} The cost of fuel per unit of power generated.

α_T Temperature coefficient of power for the PV module.

Δf Frequency deviation.

ΔP_G Power output deviation of the TPU.

η_{PV} Conversion efficiency of PV panels.

κ'_k Updated precision parameter for cluster k.

μ'_k Updated mean for cluster k, calculated based on prior information and observed data X_n.

ν'_k Updated degrees of freedom for cluster k.

π_k Prior probability of cluster k.

Ψ'_k Updated scale matrix for cluster k.

σ An emission coefficient or impact factor.

$\tau \sum_t \sum_i P^c_{i,t}$ Cumulative required power generation over time t for each generation unit i, scaled by a factor τ.

$\mathrm{St}_{\nu_k+1-\dim(X_k)}$ Student-t distribution for cluster k, with adjusted degrees of freedom given by $\nu_k + 1 - \dim(X_k)$.

C^{ASR} Revenue generated from providing ancillary services, determined by the system's regulation capabilities.

C^{EMI} The emission cost, accounting for environmental impacts and regulatory fees related to pollutant emissions.

C^{ESR} Revenue from selling electricity to end-users, based on market prices and the amount of electricity sold.

C^{FC} The fuel cost, applicable to DG units that require fuel, which is coal used in the thermal power unit of this paper.

C^{INV} The initial investment cost associated with deploying DG units and infrastructure.

C^{OM} The operation and maintenance cost required for the upkeep and operation of the system.

C^{PV}_j Investment cost for each unit type j of PV units.

C^{TPU}_j Investment cost for each unit type j of thermal power units.

C^{WT}_j Investment cost for each unit type j of wind turbines.

C_k Cluster k of similar load profiles for a 24-hour period.

$d(P_{i,t}, \mu_k)$ Distance metric between the load profile $P_{i,t}$ and the centroid μ_k of cluster k.

$E_{i,t}$	The state of charge of the ESS at node i and time t.
$E_i^{\max}$	The maximum state-of-charge limit of the ESS.
$E_i^{\min}$	The minimum state-of-charge limit of the ESS.
$f_{i,j,l}^{mt}$	Installation factor or quantity of thermal unit type j in location i and instance l.
$f_{i,j,l}^{PV}$	Installation factor or quantity of PV unit type j in location i and instance l.
$f_{i,j,l}^{WT}$	Installation factor or quantity of wind turbine type j in location i and instance l.
$f_{\mathrm{PV}}(G_t)$	A function of the solar irradiance G_t at time t.
$f_{\mathrm{WT}}(v_t)$	A function of the wind speed v_t, dependent on cut-in, rated, and cut-out wind speeds.
$G_{i,t}$	Solar irradiance at node i and time t.
G_{STC}	Standard Test Condition irradiance (1000 W/m^2).
K_f	Droop control coefficient for the ESS.
K_g	Droop control coefficient for the TPU.
N	Total number of consumers.
$N(i)$	The set of neighboring nodes connected to node i.
$P_{i,t}^{PV}$	Output power of the PV system at node i at time t.
$P_{i,t}^{WT}$	Output power of the wind turbine at node i at time t.
P_f	Power formulated based on the SOC and frequency deviation.
P_G^{actual}	Real-time output of the TPU.
P_G^{droop}	Droop-based output of the TPU.
P_m	Maximum allowable power.
P_{rated}	Rated power of the wind turbine.
P_{rec}	SOC recovery power.
P_{fess}	Primary frequency control power command of the ESS.
$P_{g,i,t}^{\mathrm{ch}}$	The charging power of the ESS at node i and time t.
$P_{g,i,t}^{\mathrm{dch}}$	The discharging power of the ESS at node i and time t.
$P_{g,i,t}^{\mathrm{PV}}$	The power output of the PV system at node i and time t.
$P_{g,i,t}^{\mathrm{TPU}}$	The active power output of the thermal generator at node i and time t.
$P_{g,i,t}^{\mathrm{WT}}$	The wind power output at node i and time t.
$P_{g,i}$	The active power generated at node i.
$P_{g,i}^{\mathrm{ch,max}}$	The maximum charging capacity of the ESS.

$P_{g,i}^{\text{dch,max}}$ The maximum discharging capacity of the ESS.

$P_{g,i}^{\text{max}}$ The maximum output limit of the thermal generator.

$P_{g,i}^{\text{min}}$ The minimum output limit of the thermal generator.

$P_{g,i}^{\text{rated}}$ The rated capacity of the wind turbine.

$P_{i,t}$ Power demand of consumer i at time t.

P_{ij} The power flow between nodes i and j.

$P_{load,i}$ The active power load at node i.

P_t Total power demand at time t.

$Q_{g,i}$ The reactive power generated at node i.

Q_{ij} The reactive power flow between nodes i and j.

$Q_{load,i}$ The reactive power load at node i.

R_{down} The ramp-down limit (rate of decrease in output) for the generator.

R_{up} The ramp-up limit (rate of increase in output) for the generator.

r_{nk} Fuzzy responsibility (or degree of membership) of cluster k for data point x_{n+1}, indicating the likelihood of the new point being assigned to cluster k.

S_{PV} Installed capacity of the PV system.

SOC_{high} High SOC threshold.

SOC_{max} Maximum SOC threshold.

SOC_{min} Minimum SOC threshold.

$T_{i,t}$ Ambient temperature at node i and time t.

T_{STC} Standard Test Condition temperature (set as 298.15 K).

$u_{ch,i,t}$ Binary variable indicating the charging status of the ESS.

$u_{dch,i,t}$ Binary variable indicating the discharging status of the ESS.

V_i The voltage at node i.

v_{in} Cut-in wind speed (minimum wind speed required to generate power).

v_{out} Cut-out wind speed (speed above which the turbine shuts down for safety).

$v_{i,t}$ Wind speed at node i and time t.

V_{max} The maximum allowable voltage level.

V_{min} The minimum allowable voltage level.

v_r Rated wind speed (speed at which the turbine generates maximum power).

1. Introduction

Modern power systems are often characterized by the integration of a large amount of renewable energy sources(RES) [1], aiming to reduce the green-house gas emissions in order to meet the target set by the Paris Agreement [2]. The UK is the first major economy legislating the target of attaining the net zero greeenhouse gas emissions by 2050 and beyond, and the first half of 2024 has seen the installation of 2GW solar power generation capacity which is more than the last 14 years combined [3]. This however has significantly reduced the system inertia, thus affecting the stability of the power grid to resist the disturbances and respond effectively to the frequency deviations [4].

Energy storage system (ESS) is considered as an effective method to compensate the fluctuations of the RESs [5]. As of the end of 2023, the global installed capacity of power grid storage projects reached 289.2 GW, marking a year-on-year growth of 21.9 % [6]. In terms of newly installed capacity, approximately 52.0 GW of power storage projects were commissioned globally in 2023, reflecting a year-on-year growth of 69.5 % [7]. Among these, the deployment of new energy storage reached a historic high of 45.6 GW. China, Europe, and the United States continued to lead the global energy storage market, collectively accounting for 88 % of the new installations, with China contributing nearly 50 % of the global total [8].

1.1. The significance of energy storage-assisted thermal power units

In contrast to many developed countries, China's resource endowment, characterized by abundant coal and limited natural gas, ensures a rich reserve for coal-fired thermal power generation(TPU). Combined with the distinctive distribution of user-side resources and a power market structure vastly different from the developed countries, integration of energy storage with coal-fired power plants has become an important research topic not only for China, but also for many other developing countries and regions where thermal power generation plants are still the dominant and affordable electricity supply technology for accessing to high quality electricity while supporting national economic growth and uptaking of more renewable generating technologies.

1) Technically, integrating energy storages with coal-fired power plants significantly enhances primary and secondary frequency regulation, providing fast and accurate grid stability support with more integration of RESs. It reduces the dynamic strain on coal-fired units, minimizing mechanical wear and carbon emissions.

2) Economically, integrating energy storage with coal-fired units has demonstrated tangible economic profits in practical applications, ESS enables coal-fired plants to participate in ancillary service markets, earning revenue through frequency regulation services. ESS increases the flexibility of coal-fired units, reducing their idle times and improving their overall energy utilization.

3) Societally, this approach provides valuable insights for policy guidance, promoting informed decisions for energy storage deployment. Additionally, it offers a new perspective and application for energy storage in power system construction, supported by strong technical and economic foundations, paving the way for sustainable and innovative energy solutions.

1.2. Literature reviews on power systems integrated with ESS

Energy storage has been widely used in the power system across the whole chain from generation, transmission, distribution to end users. For example, Yang et. al [9] highlights how user-side ESS can be strategically utilized to enhance grid reliability through effective demand response mechanisms. [10] investigates the relationship between the energy supplier and end users equipped with ESS, and explores how end users can respond to the electricity prices set by the energy suppliers and optimize their energy consumption and storage usage. Cui et.al [11] presents a structured framework to address the RES uncertainty challenge by modeling the interactions between energy providers and consumers.

Zhang et.al [12] addresses the critical issue of frequency stability in power systems using grid-connected ESS. Li et. al [13] introduces an innovative approach to managing the output power of distributed doubly-fed induction generators by integrating a grid-connected hybrid ESS and coordinating with the grid-side

converter. Xie et.al [14] explores the integration of blockchain technology into grid-side shared energy storage markets to enhance security, transparency, and efficiency in energy transactions. Khani et.al [15] highlight the importance of integrated planning and optimization in managing the complexities introduced by high shares of renewable energy, while the ESS have limited energy and power capacities, making them insufficient for handling large-scale and prolonged peak demand periods.

Jafarian et.al [16] shows that a significant reduction in power and voltage fluctuations can be achieved by integrating ESS with RES generating units. However, it does not address the frequency regulation requirements, which are critical for grid stability when integrating high-penetration renewable energy sources. Wang et.al [17] propose a preventive control strategy utilizing ESS to support RES generating units and to enhance primary frequency response. Zhang et.al [18] proposed a distributed cooperative control approach for secondary frequency regulation, enabling multiple distributed generators and ESS to work together without relying on a central controller. The paper however does not address the coordinated control of generations and energy storage systems, specifically addressing multiple objectives simultaneously, such as enhancing frequency regulation, grid flexibility, and economic performance. Liu et.al [19] developed a Generalized Predictive Control-Proportional Integral layered control strategy for energy storage integrated renewable generation systems, achieving a 30 % reduction in overshoot compared to conventional methods. Literature reviews are also concluded as Table. 1.

Table 1: Literature reviews of ESS-assisted power generations of RESs

Ref	Authors Years	ESS Types	Control strategy	Economical constraints	Pollutant emissions	Advantages	Disadvantages
[13]	Chao Li 2023	Hybrid energy storage system	Coordinated control scheme integrating HESS using a grid-side converter to enhance power stability.	High initial investment costs for HESS components and control infrastructure	Not included	The strategy enhances power stability, optimizes energy utilization, and minimizes mechanical stress.	The system's complexity and high upfront costs pose challenges for widespread adoption.
[15]	Meysam Khani 2024	ESS as interconnected entities within distribution networks	Incorporating demand-side management and coordination between transmission and distribution systems	Economic factors by demonstrating that integrating ESS can lead to significant cost reductions, distribution network costs.	The integration is expected to contribute to lowering pollutant emissions	The proposed approach enhances grid flexibility and achieves smart grid objectives.	The complexity of implementing bi-level stochastic models and ensuring coordination of distribution networks are not verified.
[16]	Masoud Jafarian 2024	Focusing on integrating efficient energy storage systems, without specifying particular ESS types.	A novel optimization and dynamic evaluation strategy is proposed to effectively integrate ESS and RES in hybrid systems.	The study addresses economic constraints by optimizing the integration strategy.	Integrating ESS with RES is expected to reduce pollutant emissions by promoting cleaner energy sources.	The proposed strategy offers improved integration of ESS and RES, leading to enhanced system performance and reliability.	The complexity of optimization models and the need for accurate dynamic evaluations.
[17]	Heng Wang 2025	Battery energy storage systems	A dynamic primary frequency response parameter adjusting scheme is proposed, enhancing frequency stability.	The integration of ESS is analyzed for its economic viability, demonstrating potential revenue generation through ancillary services .	ESS control strategy contributes to reducing reliance on fossil fuels, lowering ollutant emissions.	The proposed approach offers improved grid frequency stability and economic benefits.	The complexity of implementing advanced control strategies and ensuring seamless coordination between ESS and RESs.
[18]	Runfan Zhang 2025	Battery energy storage systems	A distributed cooperative secondary frequency control accounts for communication time delays.	Economic feasibility, considering factors such as cost-effectiveness and financial viability.	By Reducing reliance on fossil fuels, thereby lowering pollutant emissions.	Improved frequency stability and economic benefits by effectively integrating ESS and RESs.	The complexity of implementing advanced control strategies and ensuring seamless coordination between ESS and RESs.
[19]	Wanying Liu, 2024	Pumped hydro storage systems	An innovative modeling method combined with a Generalized Predictive Control PI control strategy in FR.	Economic feasibility, considering cost-effectiveness, financial viability.	Not included	The proposed approach offers improved frequency stability and economic benefits by effectively integrating PHS with RESs.	The complexity of implementing advanced control strategies.

Economic Dispatch (ED) is another critical component of modern power system operations, aiming to minimize the economic cost of electricity generation while maximizing the revenue from selling electricity [20]. By focusing on these dual objectives, ED helps develop more resilient and efficient energy systems [21]. It ensures that the generation units are dispatched in a manner that achieves economic efficiency without compromising system reliability. The integration of RES including wind and solar power, introduces significant challenges to the ED process due to their inherent variability and unpredictability [22]. Factors like wind speed, solar radiation intensity, and solar irradiance temperature are among the major contributing factors to the variability of these resources [23]. To handle this extra layer uncertainty and complexity, more sophisticated optimization models are needed for optimal power allocation while maintaining system reliability and operational efficiency [24]. Various advanced approaches have been developed for ED that incorporate RES. Li et.al [25] studied the connections between automatic generation control and ED from an optimization view, and a distributed approach to improve economic efficiency. These methods aim to optimize the dispatch of generation companies by effectively managing both the operational constraints and uncertainties of the power system [26]. Techniques such as stochastic programming, robust optimization, and hybrid models that leverage machine learning have been proposed. Nguyen et.al [27] proposed a novel robust model predictive control strategy by studying the feasibility problem considering the comparison

relations of constraint sets and Lyapunov function candidates. Furthermore, Then, the strategy is applied in Leader-Follower formation scheme in a group of followers, as well as the input-to-state stability of the proposed terminal controller and equivalent terminal region is evaluated [28]. As for the power system operations facilitating the sustainable energy transition, for example, Li et.al [29] proposed a two-tiered control framework that integrates economic considerations of energy storage lifespan with frequency regulation constraints, which optimize the operational efficiency and extend the service life of hybrid ESS. Yan et.al [30] developed a method to dynamically adjust the rotational inertia and damping coefficient of the VSG based on real-time system conditions.

Despite the latest progresses in control and dispatch of power systems with significant penetration of RES integrated with ESS, thermal power units are increasingly required to adjust their operations in response to fluctuations introduced by renewable energy generation. These adjustments include frequent cycling, rapid load changes (ramp-up and ramp-down), and frequent start-ups and shutdowns [31]. Operating away from optimal steady-state conditions reduces the thermal efficiency of power plants, leading to higher fuel consumption and emissions per unit of electricity generated [32]. To mitigate thermal damage caused by operational stress challenges, the integration of ESS has been proposed as a promising solution [33]. Guo et.al [34] showed that the coal-fired units can maintain a more stable operational profile, which improves thermal efficiency and reduces fuel consumption by charging the storage during periods of low demand or high renewable output and discharging during peak periods. The hybrid configuration also enables coal-fired power plants to participate in ancillary service markets. Su et.al [35] analyzed the impact of ESS on start-up costs and concluded that, by reducing cycling, ESS can significantly lower start-up and maintenance costs, contributing to overall cost savings. Deng et al. [36] proposed a bi-level optimization model for sizing and dispatching hybrid systems combining coal-fired power plants with various battery technologies, focusing on peak shaving applications. The cost-benefit analysis of adding ESS to coal-fired units is complex and highly dependent on the dynamic market, which limits the practical implementation of these hybrid systems. Gao et al. [37] presented a co-optimization framework for maintenance and flexibility retrofitting of coal-fired units, addressing the challenges of integrating renewable energy sources. Real-time optimization further complicates the process, as it requires sophisticated algorithms capable of handling large amounts of data and making rapid decisions.

The inherent variability of renewable energy sources also adds further uncertainty to the economic dispatch of TPU-ESS systems. Existing ED models often rely on forecasted renewable generation, which is not always accurate. Errors in forecasting can lead to suboptimal dispatch decisions, either causing unnecessary cycling of the coal unit or leading to underutilization of the ESS [38]. The development of more accurate forecasting models and robust optimization techniques is crucial for effective economic dispatch of hybrid systems. Azad et.al [39] advocated for hybrid systems combining RESs with thermal units and battery storage for sustainable grid integration. Brandt et.al [40] employed the integration of battery and thermal energy storage has been highlighted as effective for reducing ramp-up and ramp-down events, mitigating thermal fatigue, and increasing plant efficiency. Bahloul et.al [41] demonstrated that ESS enhances system reliability by providing ancillary services including frequency regulation and load balancing, contributing to grid stability. The literature review also strengthens the argument that hybrid energy systems with ESS are crucial for improving flexibility, reliability, and economic performance in a grid increasingly dominated by renewable energy [42, 43]. Other literature reviews are summarized as the following Table 2. The real-life applications have also shown promising results of thermal power plants integrated with ESS in addressing the slow response and limited frequency regulation capability of conventional coal-fired units. For example, in Lingwu, Ningxia (600 MW supercritical unit with 36 flywheel systems, 630kW/125kWh each) and Shuozhou, Shanxi (350 MW circulating fluidized bed unit with lithium battery, 6MW/6MWh, and flywheel systems,2MW/0.5MWh), all in China, energy storage has effectively improved both primary and secondary frequency regulation performance. These projects have also demonstrated significant economic benefits by generating extra revenue from ancillary service markets, making ESS deployment on the thermal power side a viable and profitable solution for enhancing power system stability and flexibility.

Table 2: Literature reviews of ESS-assisted power generations

Ref	Authors Years	ESS Types	Control strategy	Economical constraints	Pollutant emissions	Advantages	Disadvantages
[32]	Jicheng Hui, 2023	Thermal energy storage	Operational strategies that enable deep and flexible load adjustments in coal combustion processes, facilitated by the preheating effect of the TPU.	Its economic viability, considering cost-effectiveness and potential financial benefits are evaluated.	Carbon emission is analyzed.	The approach offers enhanced operational flexibility, allowing coal-fired power plants to adjust loads, accommodating fluctuations.	The technical complexity of integrating CFB preheating systems and ensuring seamless operation within existing plant infrastructures.
[35]	Pengfei Su, 2023	Thermal storage system	A multi-objective optimization model balance electricity costs, and emissions.	Economic implications, demonstrating significant reductions in electricity and emission costs, with electricity costs reduced.	Emission costs sharply reduced	The approach offers enhanced operational flexibility, improved economic performance.	Advanced scheduling models and integration of plant operations.
[44]	Yansong Zhu, 2024	Hybrid energy storage systems, combining batteries and flywheels.	Advanced energy management and operation strategies for HESS, aiming to enhance the regulation capabilities of TPUs under AGC.	The economic implications of implementing HESS, addressing cost-effectiveness and financial viability.	Not included.	The integration of HESS enhances the AGC performance of TPUs leading to improved grid stability and reliability.	Managing hybrid systems and the need for investments, which pose operational and financial hurdles.
[45]	Shiye Yan, 2024	Batteries and thermal storage	A two-stage optimization framework is proposed, focusing on coordinating ESS and implementing deep peak shaving regulation.	Economic factors including operational costs and capital investments in ESS and thermal generator upgrades.	The study aims to reduce reliance on fossil fuels.	The proposed approach offers improved grid flexibility, better accommodation of RES.	The initial capital costs of ESS deployment and control mechanisms.
[46]	Yongli Wang, 2024	Virtual energy storage characteristics of heating networks.	Optimization techniques that exploit the weak equilibrium characteristics to address high-frequency fluctuations.	Not included	The proposed strategies aim to decrease reliance on fossil fuels, thereby reducing emissions.	The approach enhances stability of integrated energy systems.	The complexity of modeling and controlling virtual energy storage dynamics and ensuring.
[47]	Ying Zhu, 2024	Pumped storage systems.	An environmental and economic scheduling approach that prioritizes the operation of thermal units based on energy-saving and emission-reduction principles.	Minimizing operational costs by optimizing the dispatch of thermal units and maximizing the wind energy.	The strategy seeks to reduce overall emissions.	The approach improves the accommodation rate of wind power, reduces output fluctuations, and lowers scheduling costs.	Implementing priority-based scheduling and ensuring the reliability of the integrated system.
[48]	Runjun Qin, 2025	Flywheel energy storage systems	The configuration and optimal dispatch strategies of the TPU-FESS system.	The study evaluates the economic implications of integrating FESS with TPUs, analyzing the effects on the economics of a regional power dispatch system.	The study suggests potential reductions in pollutant emissions due to efficient operation and better accommodations.	The integration of FESS with TPUs is shown to improve the regulating capacity of TPUs.	The initial investment costs associated with FESS implementation and the need for technical adaptations to existing TPU infrastructure.

1.3. Motivation and Contributions

The literature reviews have suggested that limited researches have been accomplished so far to assess how thermal units integrated with ESS can support power grid frequency regulation and scheduling optimization while overlooked the dynamic characteristics of energy storage systems and thermal power generations under multiple timescales, as well as the economic revenue analysis. The main contributions of the paper are summarized as follows:

1) A novel thermal power unit security indicator based on transient energy transfer is developed to evaluate the power output capability and reduce mechanical wear and component degradation during the deep peak shaving process.

2) An optimal dispatch method is proposed to maximize economic benefits by balancing frequency regulation demands, as well as a coordinated control strategy of the system is designed to enhance the energy storage short-term ability while relieve the pressure of TPUs.

3) Multiple types of energy storage systems of the constructed scenario are assessed in terms of handling system uncertainties, demonstrating that storage-assisted thermal power unit system as an economical-friendly solution.

1.4. Paper organization

The paper is organized as follows. The Introduction section provides the motivation, literature review, and a summary of the main contributions of the paper. The problem formulation section is organized in section 2. Uncertainty sets are discussed followed. Section 4 presents the robust optimization and algorithm solution, and section 5 presents a case study and the results. Conclusion section summarizes the whole work and future prospects.

2. Problem Formulation

Fig. 1 outlines the schematic of a robust optimization approach proposed in this paper for dispatching a power grid with thermal units integrated with ESSs.

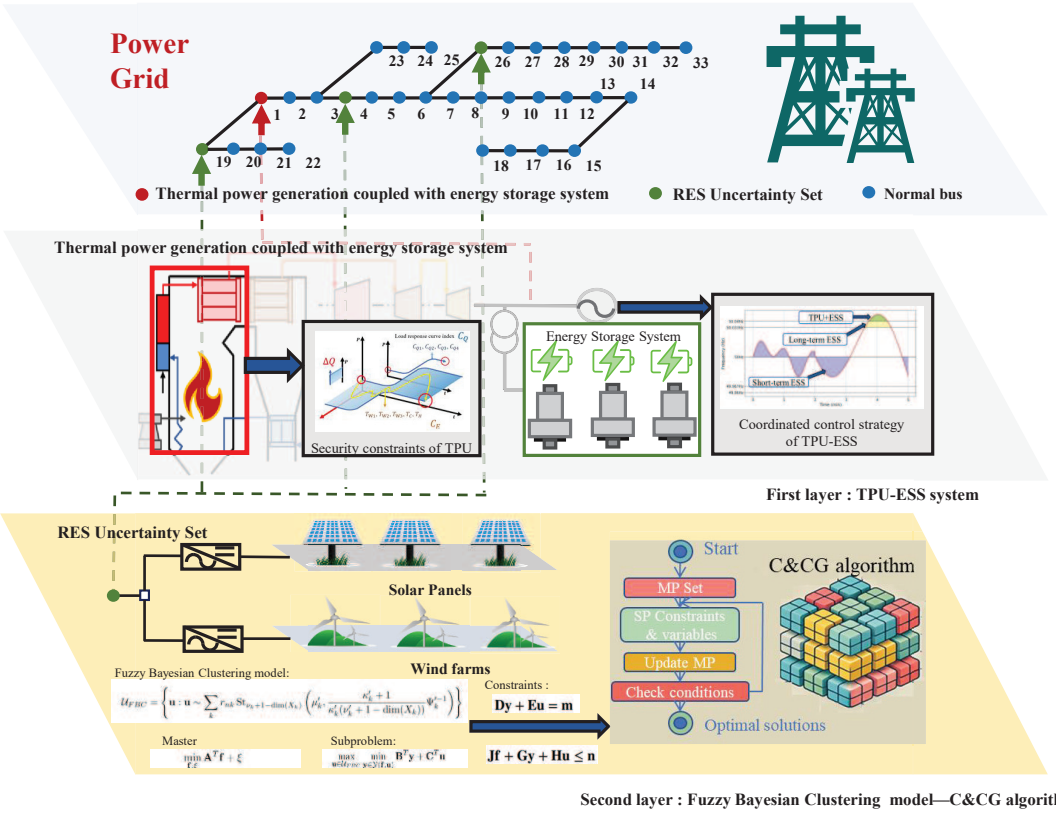

Figure 1: The robust optimization approach for dispatching a power grid with energy storage coupled thermal power units

2.1. Objective Function

Integrating RESs enables the power grid to meet demand, and the grid's ability to operate autonomously from the main grid strengthens its resilience during grid outages or natural disasters. With a diversified generation portfolio including renewable sources, the system can maintain a stable power supply for critical loads, thus enhancing overall reliability. Additionally, the ESS attached to DGs can provide backup power and frequency regulation, further stabilizing the power grid. The objective function aims to minimize the total cost or maximize net profit of the distributed energy system, accounting for various cost and revenue components. The main components include initial investment cost, operation and maintenance cost, fuel cost, emission cost, ancillary service revenue, and electricity sales revenue.Assuming the total operational period is T, the objective function can be expressed as:

$$\min_{f,P,Q,V} C^{\mathrm{INV}} + C^{\mathrm{OM}} + C^{\mathrm{FC}} + C^{\mathrm{EMI}} - R^{\mathrm{ASR}} - R^{\mathrm{ESR}} \tag{1}$$

The investment cost, operation and maintenance cost, fuel cost, emission cost, ancillary service revenue, and selling electricity revenue are expressed as followed:

$$\begin{aligned} C^{INV} = &\sum_i \sum_j \sum_l inv^{TPU} f_{i,j,l}^{TPU} C_j^{TPU} + \sum_i \sum_j \sum_l inv^{ESS} f_{i,j,l}^{ESS} C_j^{ESS} + \\ &\sum_i \sum_j \sum_l inv^{WT} f_{i,j,l}^{WT} C_j^{WT} + \sum_i \sum_j \sum_l inv^{PV} f_{i,j,l}^{PV} C_j^{PV} \end{aligned} \tag{2}$$

$$C^{OM} = \sum_t \sum_i \sum_j \sum_l om^{TPU} f_{i,j,l}^{TPU} C_j^{TPU} + om^{ESS} f_{i,j,l}^{ESS} C_j^{ESS} + om^{WT} f_{i,j,l}^{WT} C_j^{WT} + om^{PV} f_{i,j,l}^{PV} C_j^{PV} \quad (3)$$

where the equation computes the total operation and maintenance costs incurred for the various types of generation technologies over a specific time horizon.

$$C^{FC} = \alpha_{fc} \sum_t \sum_i P_{i,t}^{TPU} \quad (4)$$

where the fuel cost is calculated based on the power output of the traditional power generating units over time.

$$C^{EMI} = \alpha_{emi} \sigma \sum_t \sum_i P_{i,t}^{TPU} \quad (5)$$

where the formula estimates the total emission cost associated with the power generated by traditional power units.

$$R^{ASR} = \sum_t \sum_i P_{i,t} \beta_i P_{ref,t} \quad (6)$$

where the revenue from ancillary services is calculated by summing the product of power output and the ancillary service revenue factor for each bus over the time horizon.

$$R^{ESR} = \sum_t \sum_i \beta_t^m P_{i,t} \quad (7)$$

where the equation captures the revenue generated from the sale of electricity, where the market price factor varies over time. By multiplying the power output at each bus by the corresponding market price, this formula quantifies the financial returns from energy sales, which are critical for the overall profitability of power generation assets.

2.2. Constraints

These constraints collectively ensure the stable, reliable, and efficient operation of the ESS-TPU system under renewable energy uncertainties.

2.2.1. Equality Constraints

DistFlow equations are applied in this section to illustrate the equality contraints in the context of the power system. These equations ensure that the generation and consumption of electrical power are balanced at each node, accounting for the flow of power through the network. Equations can be expressed as follows:

$$P_{g,i} - P_{load,i} = \sum_{j \in N(i)} P_{ij} \quad \forall i \in \mathcal{N} \quad (8)$$

$$Q_{g,i} - Q_{load,i} = \sum_{j \in N(i)} Q_{ij} \quad \forall i \in \mathcal{N} \quad (9)$$

The voltage at each bus should be within specified bounds:

$$V_{min} \leq V_i \leq V_{max} \quad \forall i \in \mathcal{N} \quad (10)$$

2.2.2. Inequality Constraints

To achieve robust operation, constraints of the power system with diverse sources containing thermal generator, wind power, photovoltaic, and energy storage are not negligible to ensure each component operates within its capacity limits and adheres to system requirements.

1. Thermal power unit security constraints

Thermal generators must operate within defined minimum and maximum generation capacities, respecting ramping limits to ensure stable operation, and security criterion of boiler capability is considered. The output constraints for a thermal generator can be expressed as:

$$P_{g,i}^{\min} \leq P_{g,i,t}^{\mathrm{TPU}} \leq P_{g,i}^{\max} \quad \forall i, \forall t \tag{11}$$

$$\Delta P_{g,i,t}^{\mathrm{TPU}} \leq R_{\mathrm{up}} \quad \forall t \quad \text{(ramping up)} \tag{12}$$

$$\Delta P_{g,i,t}^{\mathrm{TPU}} \geq -R_{\mathrm{down}} \quad \forall t \quad \text{(ramping down)} \tag{13}$$

In [5], we illustrate the load variation process under the frequency regulation command. Three axis depict the conventional power ramp-up curve with its performance evaluated using the index C_Q, changes in thermal parameters energy flow and fuel consumption within the system, and the potential state transition path from the initial to the target state. These parameters are defined as the derived security criterion which is quantified by the index C_Q to integrate the security margins alongside the original load variation requirements. The load response curve index C_Q is determined based on the deviation between the target response curve and the actual response curve. Four sub-indices, C_{Q1}, C_{Q2}, C_{Q3}, and C_{Q4}, are defined to evaluate the curve, corresponding to adjustment time, rise time, overshoot, and steady-state error, respectively. By analyzing the performance of the target curve, the parameter calculation method for the objective function is derived. Assuming the adjustment time, rise time, overshoot, and steady-state error of the target curve are denoted as $\hat{T}_r$, $\hat{T}_s$, $\hat{M}_p$, and $\hat{e}_{ss}$, and the corresponding values of the actual curve are T_r, T_s, M_p, and e_{ss}, the relationship can be expressed as follows:

$$C_Q = \frac{1}{4} \times \left[\left(\frac{\left| \hat{T}_r - T_r \right|}{\hat{T}_r} \right)^2 + \left(\frac{\left| \hat{T}_s - T_s \right|}{\hat{T}_s} \right)^2 + \left(\frac{\left| \hat{M}_p - M_p \right|}{\hat{M}_p} \right)^2 + \left(\frac{\left| e_{ss} - \hat{e}_{ss} \right|}{\hat{e}_{ss}} \right)^2 \right] \tag{14}$$

2. Wind turbine constraints

The output of wind turbines depends on wind speed and turbine characteristics, resulting in variability. Wind power generation is constrained by available wind conditions, represented as:

$$0 \leq P_{g,i,t}^{\mathrm{WT}} \leq P_{g,i}^{\mathrm{rated}} \cdot f_{\mathrm{WT}}(v_t) \quad \forall i, \forall t \tag{15}$$

3. PV constraints

Photovoltaic generation depends on solar irradiance, which varies throughout the day. The output constraints for photovoltaic systems are:

$$0 \leq P_{g,i,t}^{\mathrm{PV}} \leq P_{g,i}^{\mathrm{rated}} \cdot f_{\mathrm{PV}}(G_t) \quad \forall i, \forall t \tag{16}$$

4. Energy storage system constraints

Energy storage systems must follow both power and energy limits. Their constraints include state-of-charge limits, charging and discharging limits, and operational constraints to ensure they contribute effectively to grid stability.

$$0 \leq P_{g,i,t}^{\mathrm{ch}} \leq u_{ch,i,t} \cdot P_{g,i}^{\mathrm{ch,max}} \quad \forall i, \forall t \quad \text{(charging)} \tag{17}$$

$$0 \leq P_{g,i,t}^{\mathrm{dch}} \leq u_{dch,i,t} \cdot P_{g,i}^{\mathrm{dch,max}} \quad \forall i, \forall t \quad \text{(discharging)} \tag{18}$$

$$E_i^{\min} \leq E_{i,t} \leq E_i^{\max} \quad \forall i, \forall t \quad \text{(state of charge)} \tag{19}$$

These constraints ensure that the generation of each type of power source remains within safe operational limits and adjusts based on resource availability, contributing to a stable and optimized power system.

The following inequality represents a constraint on the total power generation investment costs for thermal power, wind power, and photovoltaic solar power:

$$\tau \sum_{t} \sum_{i} P_{i,t}^{c} \leq \sum_{t} \sum_{i} \sum_{j} \sum_{l} f_{i,j,l}^{TPU} C_{j}^{TPU} + \sum_{i} \sum_{j} \sum_{l} f_{i,j,l}^{WT} C_{j}^{WT} + \sum_{i} \sum_{j} \sum_{l} f_{i,j,l}^{PV} C_{j}^{PV} \tag{20}$$

This constraint implies that the total required power generation, weighted by τ, must not exceed the sum of the investment costs for the thermal, wind, and PV energy sources.

3. Constraints of energy storage system

When the system frequency deviation surpasses the established dead zone, the TPU and the ESS must operate synchronously to engage in primary frequency regulation. This coordination balances generation and demand, mitigating frequency deviation effectively. Both the TPU and ESS utilize droop control for primary frequency regulation, following the droop control logic of the TPU. The droop control power command for the ESS is calculated as:

$$P_{ess} = K_f \cdot \Delta f \tag{21}$$

The droop control for both TPU and ESS is described as:

$$\begin{cases} P_v^{\text{droop}} = -K_f \cdot \Delta f \\ P_G^{\text{droop}} = -K_g \cdot \Delta f \end{cases} \tag{22}$$

The real-time power output deviation of the TPU is calculated as:

$$\Delta P_G = P_G^{\text{droop}} - P_G^{\text{actual}} \tag{23}$$

As Fig. 2 shown, frequency regulation response of different ESS. The red line represents the system frequency over time, with short-term ESS, long-term ESS, and TPU-ESS contributions marked. The short-term ESS responds first to frequency deviations below 49.967 Hz, as indicated by the shaded blue area. Long-term ESS becomes active to support longer duration deviations. The TPU+ESS integration provides additional support when the frequency deviation exceeds 50.033 Hz. This coordination ensures optimal frequency regulation and grid stability.

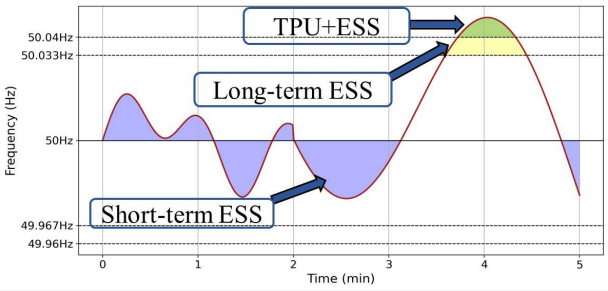

Figure 2: Coordinated dispatch strategy for TPU-ESS systems

The traditional operation of ESS is divided into two stages. Initiated when the system frequency deviation exceeds the dead zone (set to 0.033 Hz in China), the ESS engages in frequency regulation, and activated when the frequency deviation is within the dead zone, allowing the ESS to recover its SOC.

An integrated control strategy for the ESS is proposed, prioritizing frequency regulation demands while considering SOC recovery. In the operational hierarchy of the grid, frequency regulation commands are executed with the highest priority. However, when SOC recovery does not interfere with frequency regulation, the ESS can execute a combined output command:

$$P_{ess_{total}} = P_{ess_{freq}} + P_{ess_{recovery}} \tag{24}$$

This approach allows for simultaneous frequency regulation and SOC replenishment, optimizing the operational efficiency of the ESS.

The power output command of the ESS, P_f, is formulated based on the SOC and frequency deviation as:

$$P_f = \begin{cases} 0, & SOC \leq SOC_{\min} \\ min(P_F^{\text{droop}} + \Delta P_G, P_m), & SOC_{\min} < SOC \leq SOC_{\text{high}} \\ min(P_F^{\text{droop}} + \Delta P_G + P_{\text{rec}}, P_m), & SOC_{\text{high}} < SOC \leq SOC_{\max} \\ P_m, & SOC > SOC_{\max} \end{cases} \tag{25}$$

Alternatively, during charging operations, the command is:

$$P_f = \begin{cases} -P_m, & SOC \leq SOC_{\min} \\ max(P_F^{\text{droop}} + \Delta P_G + P_{\text{rec}} - P_m), & SOC_{\min} < SOC \leq SOC_{\text{high}} \\ max(P_F^{\text{droop}} + \Delta P_G, P_m), & SOC_{\text{high}} < SOC \leq SOC_{\max} \\ 0, & SOC > SOC_{\max} \end{cases} \tag{26}$$

3. Uncertainty set

3.1. Renewable Energy Source Uncertainty Set

A crucial step before the system planning is conducting a comprehensive assessment of RES availability. This is essential due to the intermittent and variable nature of RES-based DGs, which are influenced by fluctuating weather conditions. The renewable energy output for photovoltaic and wind turbine systems can be modeled with constraints that account for uncertainty in solar irradiance, temperature, and wind speed.

$$P_{i,t}^{WT} = \begin{cases} 0 & \text{if } v_{i,t} < v_{\text{in}} \text{ or } v_{i,t} > v_{\text{out}} \\ \frac{v_{i,t} - v_{\text{in}}}{v_r - v_{\text{in}}} \cdot P_{\text{rated}} & \text{if } v_{\text{in}} \leq v_{i,t} < v_r \\ P_{\text{rated}} & \text{if } v_r \leq v_{i,t} \leq v_{\text{out}} \end{cases} \tag{27}$$

$$P_{i,t}^{PV} = \eta_{PV} \cdot S_{PV} \cdot \frac{G_{i,t}}{G_{STC}} \cdot [1 - \alpha_T (T_{i,t} - T_{STC})] \tag{28}$$

3.2. Load Profile Analysis

Load profile analysis helps utilities and system operators understand the expected variations in electricity demand over a 24-hour period, allowing them to plan generation, optimize resource allocation, and ensure grid stability. A typical day-ahead load profile consists of hourly power demand values for a 24-hour period, which are generated based on various factors such as weather conditions, time of day, and historical consumption patterns. Below is representing the total demand P_t of the proposed system at any time t over the 24-hour period using the sum of individual consumer types:

$$P_t = \sum_{i=1}^{N} P_{i,t} \tag{29}$$

For clustering or segmentation of load data for day-ahead forecasting:

$$C_k = \{P_{i,t} : d(P_{i,t}, \mu_k) \leq d(P_{i,t}, \mu_j), \forall j \neq k\} \tag{30}$$

3.3. Fuzzy Bayesian Clustering Model

In this section, Fuzzy Bayesian Clustering (FBC) method is described. This method combines fuzzy clustering with Bayesian analysis, allowing each data point to partially belong to multiple clusters with associated degrees of membership. Bayesian inference further quantifies the uncertainty in cluster assignments, making FBC suitable for dynamic and uncertain data in energy systems. The FBC approach is illustrated in the accompanying figure, which highlights the load forecasting and renewable energy uncertainty set. The fuzzy Bayesian clustering steps can be illustrated as followed shown in Fig: 3.Three Gaussian-distributed clusters with specific means and covariance matrices is generated. The generated synthetic data provides a realistic foundation for testing clustering algorithms and observing how they respond to different distributions shown in Fig: 3(a). The KMeans approach is refined in subsequent steps shown in Fig: 3(b). This approach allows for overlapping clusters and reflects the uncertainty in each assignment, providing a more flexible and realistic representation of the data structure shown in Fig: 3(c).

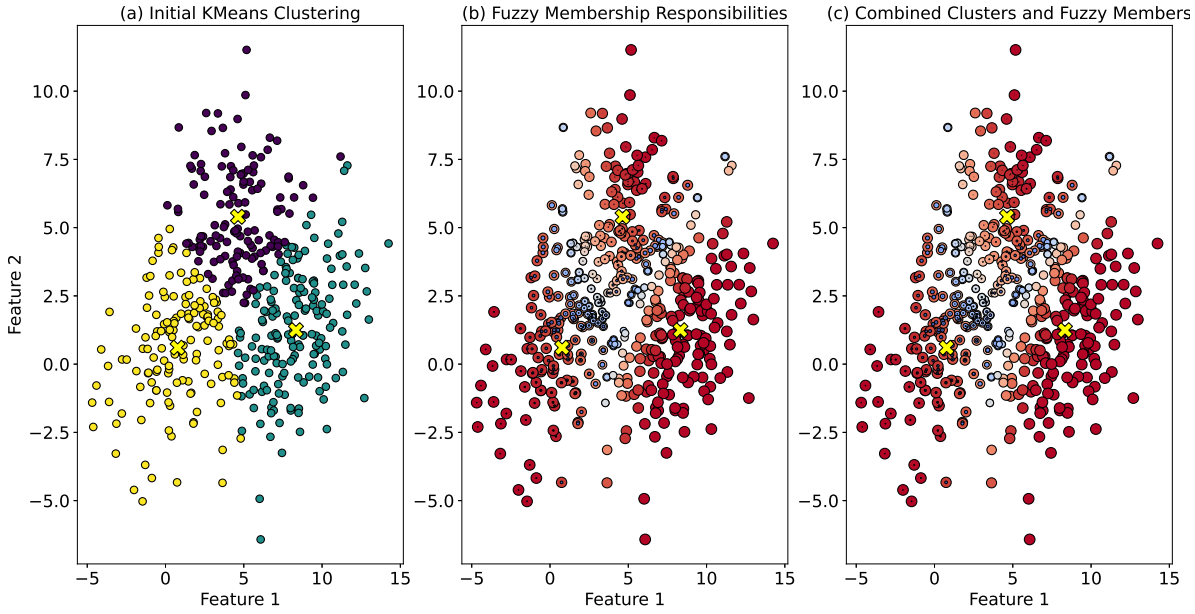

Figure 3: Visualization of the three steps in Fuzzy Bayesian Clustering

Assume a dataset $X = \{x_1, x_2, \ldots, x_N\}$ is used to be clustered into K clusters. The steps of Fuzzy Bayesian Clustering are as follows. First, Utilizing the KMeans algorithm to initialize the cluster centers $\{\mu_k\}_{k=1}^{K}$. Then, for each data point x_i, calculate its fuzzy responsibility r_{ik}, representing the degree to which x_i belongs to cluster k. The responsibility is given by:

$$r_{ik} = \frac{\pi_k \cdot p(x_i|\theta_k)}{\sum_{j=1}^{K} \pi_j \cdot p(x_i|\theta_j)} \tag{31}$$

Then, using the fuzzy responsibilities, update the cluster centers μ_k and other parameters iteratively to approach the optimal solution.

$$\mu_k = \frac{\sum_{n=1}^{N} r_{nk} \cdot x_n}{\sum_{n=1}^{N} r_{nk}} \tag{32}$$

If it is applicable, then update the cluster covariances.

$$\Sigma_k = \frac{\sum_{n=1}^{N} r_{nk} \cdot (x_n - \mu_k)(x_n - \mu_k)^T}{\sum_{n=1}^{N} r_{nk}} \tag{33}$$

Then, updated the priors.

$$\pi_k = \frac{1}{N} \sum_{n=1}^{N} r_{nk} \tag{34}$$

Finally, repeat the calculation of fuzzy responsibilities and the update of cluster centers until convergence, resulting in the final fuzzy clustering.

3.4. Formulation of FBC Uncertainty Set

The uncertainty set is constructed by capturing the probabilistic nature of data point assignments to clusters. The fuzzy membership structure is fundamental in defining the uncertainty set for robust optimization, especially when dealing with renewable energy generation, which is inherently variable and unpredictable. :

The posterior predictive distribution in FBC represents the likelihood of a new data point x_{n+1} belonging to any of the clusters k given the observed data X_n and model parameters Ξ. This distribution captures both the clustering structure and the probabilistic membership of each point across clusters.

The posterior predictive distribution for a new data point x_{n+1} is given by:

$$p(x_{n+1}|X_n, \Xi) \sim \sum_k r_{nk} \, \mathrm{St}_{\nu_k+1-\dim(X_k)} \left(\mu'_k, \frac{\kappa'_k + 1}{\kappa'_k(\nu'_k + 1 - \dim(X_k))} \Psi'^{-1}_k \right) \tag{35}$$

The uncertainty set $\mathcal{U}$ in FBC is then constructed by combining the posterior predictive distributions of each cluster, weighted by the fuzzy memberships. This set represents the range of potential outcomes for x_{n+1}, encapsulating the full scope of variability in the model based on the observed data. Mathematically, the uncertainty set $\mathcal{U}$ can be defined as:

$$\mathcal{U} = \left\{ x : x \sim \sum_k r_{nk} \, \mathrm{St}_{\nu_k+1-\dim(X_k)} \left(\mu'_k, \frac{\kappa'_k + 1}{\kappa'_k(\nu'_k + 1 - \dim(X_k))} \Psi'^{-1}_k \right) \right\} \tag{36}$$

This representation means that any point x in the uncertainty set is drawn from the mixture distribution specified by the posterior predictive distribution. Each cluster k contributes to the uncertainty set proportionally to its responsibility r_{nk} for the data point x_{n+1}. High responsibility values indicate that a cluster has a strong influence over the point's membership, while low values indicate a weaker influence. This fuzzy membership enables the uncertainty set to accommodate points that belong to multiple clusters, effectively capturing the variability of renewable output patterns.To guarantee tractability and robust feasibility in the presence of uncertainty modeled by FBC, we derive a confidence-bound-based outer approximation of the uncertainty set $\mathcal{U}$ in Eq. (36). Specifically, the predictive posterior for each cluster k is a multivariate Student-t distribution, from which we extract a high-confidence interval, $\left[\mu'_k - t_{\alpha/2,\nu'_k} \cdot \sigma_k,\ \mu'_k + t_{\alpha/2,\nu'_k} \cdot \sigma_k\right]$, with $\sigma_k = \sqrt{\frac{\kappa'_k+1}{\kappa'_k(\nu'_k+1-\dim(X_k))} \cdot \Psi'_k}$.

In this construction, each cluster is represented by a Student-t distribution with parameters specific to that cluster. The Student-t distribution is particularly useful here because it is robust to outliers and can accommodate a variety of data distributions. The degrees of freedom $\nu_k + 1 - \dim(X_k)$ control the shape of the distribution, allowing it to capture the inherent variability in renewable output for that cluster. The mean μ'_k represents the expected value of data points in cluster k, while the precision κ'_k scales the Student-t distribution, influencing the spread around the mean. A higher precision κ'_k implies more confidence in the mean estimate. The degrees of freedom ν'_k affect the tail behavior of the distribution, with higher values leading to a more Gaussian-like shape and lower values resulting in heavier tails, accommodating more variability. Finally, the scale matrix Ψ'_k adjusts for variability in multiple dimensions, making the model robust to multivariate uncertainty.

The constructed uncertainty set $\mathcal{U}$ can now be applied in robust optimization to improve the resilience of the system. This uncertainty set allows the optimization model to consider a variety of possible outcomes for renewable output and make decisions that remain feasible under different scenarios. For instance, in

energy dispatch, the robust optimization framework can look at the lower end of the uncertainty set to prepare for worst-case scenarios, ensuring backup from thermal or stored energy is available when renewable output is low. Conversely, the upper bounds of the uncertainty set represent favorable conditions where renewable generation is high, enabling the dispatch model to minimize thermal generation and utilize storage to capture excess renewable energy. By using the full range of the uncertainty set, the optimization model can dynamically adjust decisions based on the probabilistic distribution of renewable energy, balancing the trade-off between cost and reliability.

The final form of the uncertainty set $\mathcal{U}$ can be represented as a distribution over possible future values, capturing the entire range of cluster-based predictions from FBC:

$$\mathcal{U} = \left\{ x \in \mathbb{R}^d : p(x|X_n, \Xi) \sim \sum_{k=1}^{K} r_{nk} \, \mathrm{St}_{\nu_k+1-\dim(X_k)} \left(\mu'_k, \frac{\kappa'_k + 1}{\kappa'_k(\nu'_k + 1 - \dim(X_k))} \Psi'^{-1}_k \right) \right\} \tag{37}$$

where d is the dimensionality of the data space. This set represents all possible outcomes x that are consistent with the fuzzy-clustered predictive distribution, covering both typical and extreme values. In Fuzzy Bayesian Clustering, the uncertainty set $\mathcal{U}$ is constructed by combining cluster-specific Student-t distributions weighted by fuzzy memberships. This set provides a robust representation of potential renewable energy outputs, accommodating uncertainty in both cluster assignment and future data points. By integrating this uncertainty set into robust optimization, energy systems can make informed decisions that remain effective under a range of future conditions, enhancing the resilience and reliability of the power grid in the face of renewable variability.

4. Robust Optimization methodology

4.1. Robust Power Grid Dispatching Model

A two-stage robust optimization framework is proposed in this paper for power system dispatching considering the integration of DG units, renewable energy sources, and storage. The objective is to handle the uncertainties inherent in RES generation and load demand.These intervals reflect the marginal variability captured by each cluster. Then, the total uncertainty set is conservatively approximated by aggregating all cluster-wise bounds according to the fuzzy membership weights r_{nk}. This forms a bounding region $\bar{\mathcal{U}}$ in either box-type or ellipsoidal form, which is then used in the outer maximization in:

$$\min_{\mathbf{f}\in\mathcal{F}} \left(\mathbf{A}^T\mathbf{f}\right) + \max_{\mathbf{u}\in\bar{\mathcal{U}}} \min_{\mathbf{y}\in\mathcal{Y}(\mathbf{f},\mathbf{u})} \left(\mathbf{B}^T\mathbf{y} + \mathbf{C}^T\mathbf{u}\right). \tag{38}$$

s.t.

$$\mathbf{D}\mathbf{y} + \mathbf{E}\mathbf{u} = \mathbf{m} \tag{39}$$

$$\mathbf{J}\mathbf{f} + \mathbf{G}\mathbf{y} + \mathbf{H}\mathbf{u} \leq \mathbf{n} \tag{40}$$

where, in the optimization model, $\mathbf{f}$ represents the vector of all first-stage decision variables, which includes $\mathbf{f}^{\mathrm{TPU}} = [f_{\mathrm{TPU},i,j,l}]$, $\mathbf{f}^{\mathrm{WT}} = [f_{\mathrm{WT},i,j,l}]$, and $\mathbf{f}^{\mathrm{PV}} = [f_{\mathrm{PV},i,j,l}]$ for all i, j, and l. The binary set $\mathbf{F} = \{0,1\}^{3\times I_b \times J_g \times L_i}$ imposes constraints on the L_i increments of the J_g types of thermal power units, wind turbine, and photovoltaic units in a power grid with I_b candidate buses. The matrices $\mathbf{A}$ and $\mathbf{J}$ correspond to the parameters for the binary variables $\mathbf{f}$. Meanwhile, in the second stage, $\mathbf{U}$ represents the uncertainty set for the vector $\mathbf{u}$, which includes the wind and solar power output $\boldsymbol{\omega}_{\mathrm{WT}} = [\omega_{\mathrm{WT},i,j,l,t}]$, $\boldsymbol{\omega}_{\mathrm{pv}} = [\omega_{\mathrm{PV},i,j,l,t}]$ for all i, j, l, and t, and the active and reactive load demand $\mathbf{P}_c = [P_{c,i,t}]$, $\mathbf{Q}_c = [Q_{c,i,t}]$ for all i and t. The matrices $\mathbf{C}$, $\mathbf{E}$, and $\mathbf{H}$ represent the parameters for the uncertain variables $\mathbf{u}$. The set $\mathbf{Y}(\mathbf{f},\mathbf{u})$ represents the feasible region for the vector of other continuous variables $\mathbf{y} = [\mathbf{P}_{\mathrm{TPU}}; \mathbf{P}_{\mathrm{WT}}; \mathbf{P}_{\mathrm{PV}}; \mathbf{Q}_{\mathrm{TPU}}; \mathbf{Q}_{\mathrm{WT}}; \mathbf{Q}_{\mathrm{PV}}; \mathbf{P}; \mathbf{Q}; \mathbf{V}]$, where $\mathbf{P}_{\mathrm{TPU}} = [P_{\mathrm{TPU},i,t}]$, $\mathbf{P}_{\mathrm{WT}} = [P_{\mathrm{WT},i,t}]$, $\mathbf{P}_{\mathrm{PV}} = [P_{\mathrm{pv},i,t}]$, $\mathbf{Q}_{\mathrm{TPU}} = [Q_{\mathrm{TPU},i,t}]$, $\mathbf{Q}_{\mathrm{WT}} = [Q_{\mathrm{WT},i,t}]$, $\mathbf{Q}_{\mathrm{PV}} = [Q_{\mathrm{PV},i,t}]$, $\mathbf{Q} = [Q_{i,t}]$, and $\mathbf{V} = [V_{i,t}]$ for all i and t, and $\mathbf{P} = [P_{1+,t}, P_{1-,t}, P_{i,t}]$ for all i and t,

where $i \neq 1$. The corresponding parameter matrices in the objective function and inequality constraints are represented by $\mathbf{B}$ and $\mathbf{G}$. The vectors $\mathbf{m}$ and $\mathbf{n}$ represent the remaining scalars in the equality and inequality constraints, respectively.

4.2. Robust Methods for Solving Power Grid Optimal Dispatching

In the two-stage optimization problem formulation subsection, the uncertainty set is defined by the posterior predictive distribution capturing the range of renewable outputs based on historical and forecast data. The problem solving method is illustrated in Fig. 4.

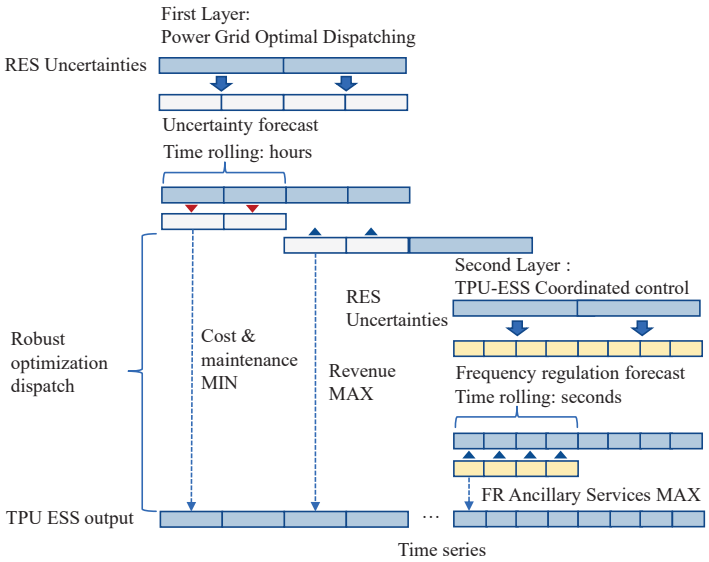

Figure 4: The proposed two-stage robust optimization procedure

4.2.1. Model Formulation with FBC-Based Uncertainty Set

The first stage of the optimization problem focuses on making initial configuration decisions for the power grid, such as selecting and placing power generation units. The second stage then uses the FBC-based uncertainty set to account for RES variability in dispatching and operational decisions.

The robust optimization model can be formulated as follows:

$$\min_{\mathbf{f}\in\mathcal{F}} \mathbf{A}^T\mathbf{f} + \xi \tag{41}$$

subject to:

$$\xi \geq \mathbf{B}^T\mathbf{y} + \mathbf{C}^T\mathbf{u} \quad \forall \mathbf{y} \in \mathcal{Y}(\mathbf{f}, \mathbf{u}) \tag{42}$$

$$\mathbf{D}\mathbf{y} + \mathbf{E}\mathbf{u} = \mathbf{m} \tag{43}$$

$$\mathbf{J}\mathbf{f} + \mathbf{G}\mathbf{y} + \mathbf{H}\mathbf{u} \leq \mathbf{n} \tag{44}$$

where, $\mathbf{f}$ represents the vector of first-stage decision variables, which includes decisions regarding the configuration of thermal power units, wind turbines, and photovoltaic units. The second-stage decision variables, $\mathbf{y}$ and $\mathbf{u}$, represent the operational decisions and uncertain parameters, respectively, where $\mathbf{u}$ is defined by an uncertainty set based on the FBC model.

4.2.2. FBC-Based Uncertainty Set Definition

Using the FBC model, we construct a probabilistic uncertainty set $\mathcal{U}_{FBC}$, which accounts for the variability in wind and solar outputs. This set is defined as a weighted mixture of cluster-specific distributions derived from the posterior predictive distribution in FBC:

$$\mathcal{U}_{FBC} = \left\{ \mathbf{u} : \mathbf{u} \sim \sum_k r_{nk} \, \mathrm{St}_{\nu_k+1-\dim(X_k)} \left(\mu'_k, \frac{\kappa'_k + 1}{\kappa'_k(\nu'_k + 1 - \dim(X_k))} \Psi'^{-1}_k \right) \right\} \tag{45}$$

where each cluster k represents a distinct renewable output scenario, and r_{nk} represents the fuzzy membership of the scenario.

4.2.3. Two-Stage Optimization considering FBC Uncertainty Set

The first stage solves for the optimal power grid configuration under different renewable scenarios, while the second stage adjusts operational decisions based on the uncertainty set $\mathcal{U}_{FBC}$.

The optimization can be split into a master problem (MP) and subproblems (SP) that correspond to different scenarios within the FBC-based uncertainty set.

1. Master Problem (MP)

$$\min_{\mathbf{f},\xi} \mathbf{A}^T\mathbf{f} + \xi \tag{46}$$

subject to:

$$\xi \geq \mathbf{B}^T\mathbf{y} + \mathbf{C}^T\mathbf{u} \quad \forall \mathbf{y} \in \mathcal{Y}(\mathbf{f}, \mathbf{u}),\, \mathbf{u} \in \mathcal{U}_{FBC} \tag{47}$$

$$\mathbf{D}\mathbf{y} + \mathbf{E}\mathbf{u} = \mathbf{m} \tag{48}$$

$$\mathbf{J}\mathbf{f} + \mathbf{G}\mathbf{y} + \mathbf{H}\mathbf{u} \leq \mathbf{n} \tag{49}$$

The result of the master problem is a relaxed solution that provides a lower bound LB for the optimization. This solution is then passed to the subproblems to evaluate its feasibility under different scenarios within the uncertainty set.

2. Subproblem (SP)

For each scenario k, represented by cluster k in the FBC uncertainty set, we solve a subproblem to identify the worst-case scenario within the uncertainty set. This ensures the feasibility of the first-stage decision $\mathbf{f}$ under the worst-case realizations of renewable output.

$$\max_{\mathbf{u}\in\mathcal{U}_{FBC}} \min_{\mathbf{y}\in\mathcal{Y}(\mathbf{f},\mathbf{u})} \mathbf{B}^T\mathbf{y} + \mathbf{C}^T\mathbf{u} \tag{50}$$

subject to:

$$\mathbf{D}\mathbf{y} + \mathbf{E}\mathbf{u} = \mathbf{m} \tag{51}$$

$$\mathbf{J}\mathbf{f} + \mathbf{G}\mathbf{y} + \mathbf{H}\mathbf{u} \leq \mathbf{n} \tag{52}$$

This subproblem evaluates the upper bound UB_k for each scenario and adjusts the feasible region by adding cuts to exclude infeasible solutions. The optimality cuts, which are associated with the worst-case uncertain variables, are then added to the master problem. To solve the challenging bi-level "max-min" subproblem using standard solvers, we formulate the KKT optimality conditions as follows:

$$\mathbf{D}\mathbf{y} + \mathbf{E}\mathbf{u} = \mathbf{m} \tag{53}$$

$$\mathbf{B}^T + \gamma^T\mathbf{G} + \delta^T\mathbf{D} = 0 \tag{54}$$

$$\mathbf{J}\mathbf{f} + \mathbf{G}\mathbf{y} + \mathbf{H}\mathbf{u} \leq \mathbf{n} \tag{55}$$

$$\gamma^\top(\mathbf{n} - \mathbf{Jf} - \mathbf{Gy} - \mathbf{Hu}) = 0 \tag{56}$$

Constraint (56) represents the complementary slackness condition, indicating that either γ or $(\mathbf{n} - \mathbf{Jf} - \mathbf{Gy} - \mathbf{Hu})$ should be zero. Using the Big-M method, we can transform this condition along with Constraint (55) into the following mixed-integer linear constraints:

$$0 \leq \mathbf{n} - \mathbf{Jf} - \mathbf{Gy} - \mathbf{Hu} \leq \mathbf{M}\sigma \tag{57}$$

$$0 \leq \gamma \leq \mathbf{M}(1 - \sigma) \tag{58}$$

where $\mathbf{M}$ is a sufficiently large constant and σ is a binary variable. The KKT conditions are sufficient when the subproblem is convex. The complete set of constraints now comprises (53), (54), (57), and (58).

4.2.4. Solution Procedure

The solution procedure involves iteratively solving the master problem and subproblems, refining the uncertainty set $\mathcal{U}_{FBC}$ based on the worst-case scenarios identified in each iteration. This approach is summarized as follows:

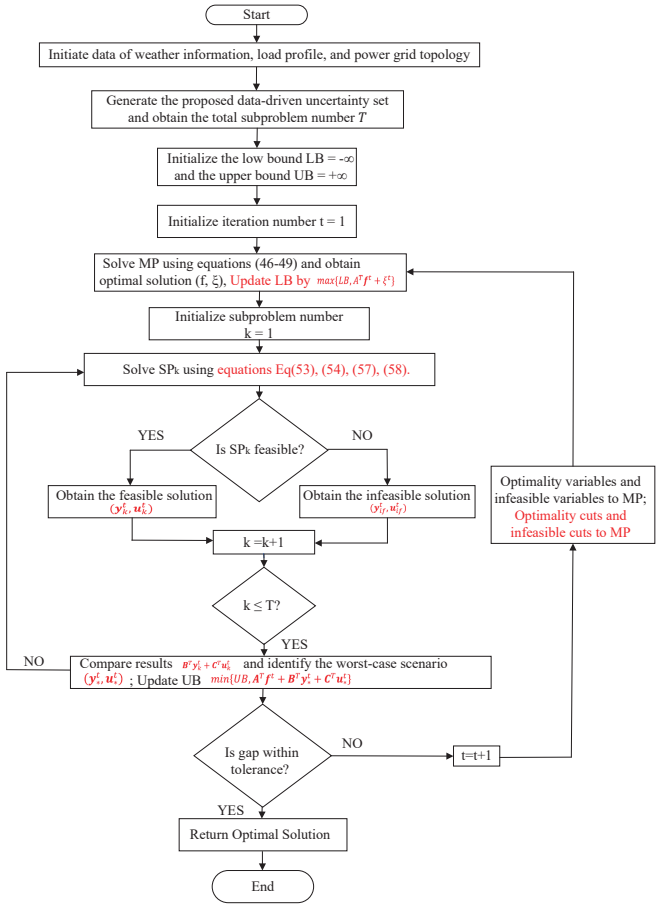

Figure 5: Flowchart of the solution algorithm for FBC-based framework

- **Step 0**: Set initial lower bound $LB = -\infty$ and upper bound $UB = +\infty$. Define tolerance ϵ and set iteration $t = 1$.

- **Step 1**: Solve the master problem (MP) and obtain the tentative solution $(\mathbf{f}^t, \xi^t)$. Update the lower bound LB=$\max\left\{LB, A^\top \mathbf{f}^t + \xi^t\right\}$.
- **Step 2**: Solve each subproblem SP_k using $\mathbf{f}^t$ to find the optimal scenario outcome $Q_k^t = (\mathbf{y}_k^t, \mathbf{u}_k^t)$ under uncertainty.
- **Step 3**: Compare Q_k^t for all $k = 1, 2, ..., T$, identifying the worst-case scenario $Q_*^t = (\mathbf{y}_*^t, u_*^t)$ and infeasible scenario set $\mathbf{Q}_{if}^t = (\mathbf{y}_{if}^t, \mathbf{u}_{if}^t)$. Update upper bound as $UB = \min\left\{UB, \mathbf{A}^\top \mathbf{f}^t + \mathbf{B}^\top \mathbf{y}_*^t + \mathbf{C}^\top \mathbf{u}_*^t\right\}$.
- **Step 4**: Check the gap between UB and LB, $GAP = \left|\frac{UB-LB}{UB}\right|$. If the gap is below ϵ, terminate the procedure. Otherwise, update the MP by adding new variables $\mathbf{y}_*^t$ and $\mathbf{y}_{if}^t$ and corresponding optimal cuts $(\mathbf{D}\mathbf{y}_*^t + \mathbf{E}\mathbf{u}_*^t = \mathbf{m})$ and $(\mathbf{J}\mathbf{f} + \mathbf{G}\mathbf{y}_*^t + \mathbf{H}\mathbf{u}_*^t \leq \mathbf{n})$, while infeasible cuts $(\mathbf{D}\mathbf{y}_{if}^t + \mathbf{E}\mathbf{u}_{if}^t = \mathbf{m})$ and $(\mathbf{J}\mathbf{f} + \mathbf{G}\mathbf{y}_{if}^t + \mathbf{H}\mathbf{u}_{if}^t \leq \mathbf{n})$. Update $t = t + 1$ and go back to step 1.

By iteratively refining the solution, this approach ensures the robustness of power grid planning decisions against the variability in renewable energy output, as represented by the FBC-based uncertainty set, the algorithm process is shown in Fig. 5.

5. Case Study: Economic Optimization and frequency regulation of the Power grid

In the section, a modified IEEE 33-bus system is used as the test power grid to validate the distributed generation network dispatching design with the FBC-C&CG framework. To find the optimal DG mix, the proposed methodologies will be analyzed under various conditions.

5.1. The Power Grid Description

The single-line topology of the system is shown in Fig. 1. The total basic load is 650 MW and 315 MVAR. In the figure, the blue nodes are denoted as normal buses where load demands are connected. The green nodes are three possible sites (bus 4, 19, and 26) that not only have load demands connected but also can be chosen to install DG units due to geographic advantages. Each possible site could install either wind generation, PV panels. The red node is the energy storage system coupled with thermal power unit (bus 1), and this is the main regulation elements for the system to resist fluctuations of the RES uncertainties.

The capital costs for thermal power plants, wind turbine, and photovoltaic generation units are \$2293/kVA, \$1882/kVA, \$4004/kVA, respectively. The O&M costs of the three DG units are \$0.012/kWh, \$0.01/kWh, and \$0.01/kWh,respectively. For thermal power unit, the fuel cost and emission penalty costs are \$0.63/kWh and \$0.02 kg/kWh, respectively. The emission factor is \$0.003 kg/kWh. For energy storage system, this study considers a capital cost of \$2000/kWh and a round-trip efficiency of 85% for flywheel energy storage systems, and a capital cost of \$400/kWh with 90% efficiency for lithium-ion battery energy storage systems. The O&M cost is estimated at \$0.004/kWh for flywheels, while the operational cost of batteries is assumed negligible due to minimal maintenance requirements.

The system is modeled on a 600 MW coal-fired thermal power plant in Lingwu, Ningxia Province, China which serves as the primary baseload generation unit, which can be shown in Table. 3. The thermal power unit ensures grid stability by providing consistent energy output, especially during periods of low renewable generation. Meanwhile, the wind turbines and PV modules operate in parallel to reduce dependency on fossil fuels and contribute to peak power demands. The base configuration which is located in Lingwu, Ningxia, employs 36 flywheel energy storage units, each with a power rating of 625 kW and a storage capacity of 153 kWh. Flywheel energy storage system (FESS) is applied for addressing transient fluctuations in wind and solar output, ensuring smoother grid operation. In contrast, the other configuration uses battery energy storage systems with the same power rating of 625 kW but a significantly higher storage capacity of 45 MWh, enabling extended-duration energy support.

Table. 4 summarizes the characteristics of the wind turbines and photovoltaic modules used in the hybrid renewable energy system. For wind turbines, the parameters include rated power, cut-in speed, rated speed, and cut-out speed, with a configuration of 3 MW rated power, 4 m/s cut-in speed, 10 m/s rated speed, and

Table 3: Characteristics of available TPU, ESS.

Thermal power unit parameters		**Type I**	**Type II**	**Type III**
Parameters	Rated power (MW)	600	600	600
Energy storage system parameters		**Type I**	**Type II**	**Type III**
Parameters	Rated Power (MW)	7.5	22.5	22.5
	Energy Capacity (MWh)	1.83	5.5	45

25 m/s cut-out speed. These specifications ensure efficient operation under a range of wind conditions.For PV modules, the parameters include peak power, open circuit voltage, short circuit current, voltage and current at the maximum power point, voltage temperature coefficient, current temperature coefficient, and nominal cell operating temperature. The PV modules are optimized with a peak power of 50 W and a nominal cell operating temperature of 43°C to perform reliably under high-temperature conditions.

Wind turbines and PV modules are strategically deployed at nodes 4, 19, and 26 within the power network. The total installed capacity is 300 MW for wind turbines and 200 MW for PV modules. This configuration takes advantage of local wind and solar resources while minimizing transmission losses and ensuring stable integration into the grid.

Table 4: Characteristics of Wind Turbine and PV Module Parameters

Wind Turbine Parameters		**Value**
Parameters	Rated power (MW)	3
	Cut-in speed (m/s)	4
	Rated speed (m/s)	10
	Cut-out speed (m/s)	25
PV Module Parameters		
Parameters	Peak power (W)	50
	Open circuit voltage (V)	55.50
	Short circuit current(A)	1.80
	Voltage at maximum power point (V)	38.00
	Current at maximum power point (A)	1.32
	Voltage temperature coefficient (mV/°C)	194.00
	Current temperature coefficient (mA/°C)	1.40
	Nominal cell operating temperature (°C)	43.00

5.2. Comparison Results of Optimization for the Power Grid

5.2.1. Analysis of RES Uncertainty Set

This analysis utilizes 10 days of weather data from China mainland, to model renewable energy generation at candidate buses 4, 19, and 26. Each station provides wind speed and solar radiation data corresponding to its assigned bus. The load profiles for all connected loads are sourced from the State Grid Shandong Electric Research Institute. The uncertainties in the system are modeled to account for wind turbine parameters, PV module parameters, and load variations across the three buses. Specifically, the uncertainty dimensions include contributions from wind turbines (3×3), PV modules (3×3), and load profiles (1), resulting in a total uncertainty dimension of 19.

The clustering results for normalized wind and solar data over a 10-day period are shown in Fig. 6. The solar output exhibits a clear diurnal pattern, with peak values occurring in the day time. During nighttime, the output is nearly zero. However, the peak values vary across different days, highlighting the randomness and uncertainty in solar output. In contrast to solar energy, wind output shows significantly higher variability and does not follow a clear diurnal pattern. The fluctuations in wind output are more random throughout the day, reflecting a greater degree of uncertainty.

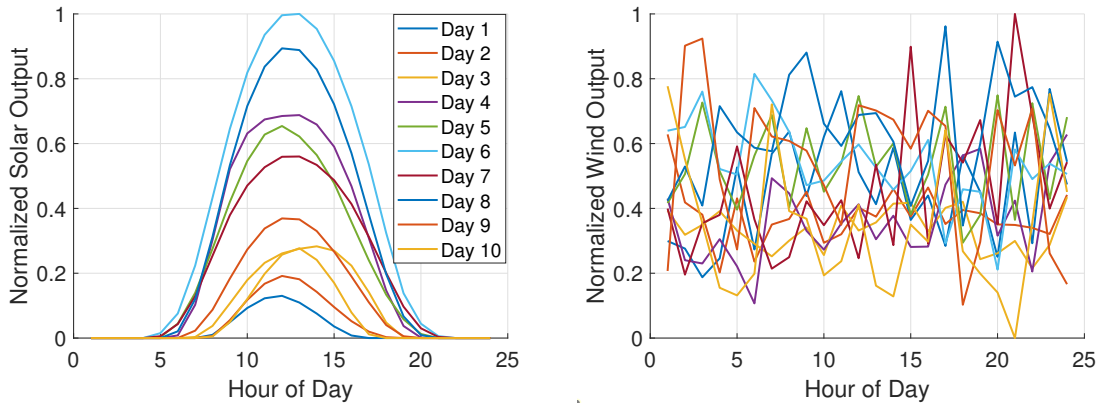

(a) Normalized solar data across 10 days (b) Normalized solar data across 10 days

Figure 6: Normalized RES Data Across 10 Days.

Fig. 7 illustrates the results of clustering normalized wind and solar data over a 10-day period using the Fuzzy Bayesian Clustering method. The figure provides insights into how wind and solar energy outputs can be categorized into distinct operating patterns, aiding in the analysis of renewable energy systems. The clustering process aimed to group the data into meaningful categories, with each cluster representing a specific range of wind and solar power generation levels. This analysis enables the characterization of renewable energy variability and supports efficient energy management strategies. The three subplots in the figure illustrate different stages of the clustering process. Subplot (a) shows the initial clustering performed using the KMeans algorithm, where each data point is assigned to a single cluster. This initial step categorizes the data into three distinct clusters, representing low, medium, and high wind-solar power output conditions, with black crosses marking the cluster centers. Subplot (b) transitions to the fuzzy clustering step, which provides a probabilistic measure of each data point's membership in the clusters. In this subplot, darker points indicate strong associations with a single cluster, while lighter points reflect shared memberships across multiple clusters, capturing the transitional nature of the data. Subplot (c) combines these results, presenting the final clustering outcome that integrates the hard clustering of KMeans with the fuzzy memberships to produce a refined representation of the wind-solar patterns.

Clustering in subplot (a) corresponds to periods of low wind and solar output, typically observed during nighttime or under overcast weather conditions. Clustering in subplot (b) represents moderate power output, such as during early morning or late afternoon, when either wind speeds or solar radiation is partially available. Clustering in subplot (c) captures high power generation scenarios, reflecting optimal wind and solar conditions during the day. These findings are instrumental in optimizing hybrid renewable energy systems by informing decisions on energy storage allocation, grid integration strategies, and the efficient management of variable renewable energy resources.

5.2.2. Comparison Under Different Confidence Levels

Once the uncertainty sets are ready, the proposed modified C&CG algorithm will be used to solve the proposed problem. All the simulation results are implemented with CPLEX 12.8.0 using a computer with an Inter(R) Core(TM) i7-12700H CPU at 4.7 GHz.

Figure 8 visualizes the distribution of costs for 3 distinct categories, which include First stage cost and Total cost for three different types which are shown in Table 4. The three types represent different cost structures or scenarios, and each type includes both the First stage cost, which represents the initial investments for all generations, and the Total cost, which combines the initial costs, operation cost and revenue of the generation dispatching for 20 years. It illustrats the cost analysis of different energy storage scenarios under varying confidence levels. The x-axis categorizes the storage scenarios into three types (Type I, Type II, and Type III), further divided into *First Stage Cost* and *Total Cost* for each type. The confidence

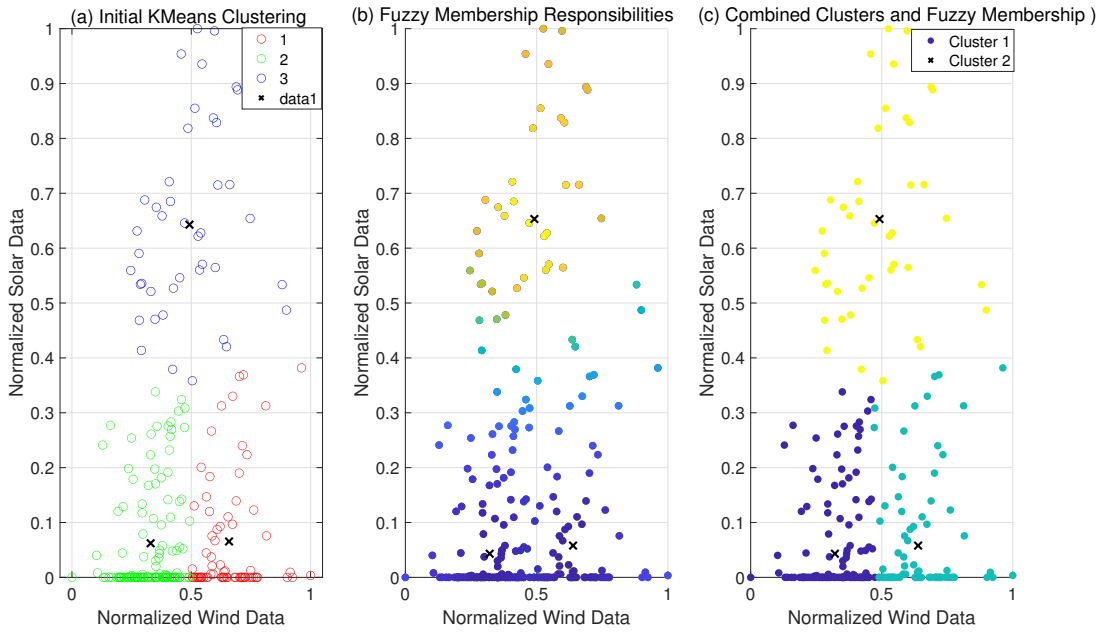

Figure 7: Normalized RES Data Across 10 Days

levels ranging from 0.5 to 0.95, which reflect the uncertainty tolerance in the optimization problem, reveals that as the confidence level increases, both the first stage and total costs generally rise, indicating higher expenses for robust planning under stricter uncertainty constraints. Across all scenarios, the total cost is consistently higher than the first stage cost, reflecting the inclusion of penalty costs for power shortages or operational adjustments in the total cost. Notably, Type II exhibits higher costs compared to Type I and Type III, indicating its potentially higher investment and operational requirements.

In this section, Type II is used as an example. From the bar chart in Fig. 8, it can be observed that when a storage capacity of 22.5 MW is configured, the reduction in total cost is the most significant. Although Type III exhibits lower initial costs, the total benefits decrease over the usage period, implying that Type II is the most effective storage configuration for long-term performance. Therefore, Type II is selected to illustrate the optimization process.

The optimization process begins by defining the objective function, which minimizes the total cost including both the first stage investment cost and the second stage operational cost. This optimization is solved under varying confidence levels to account for uncertainties in energy production and demand. The iteration proceeds using a C&CG method until convergence is achieved.

The optimization results are presented in Table. 5. For Type II, the total cost effectively decreased, and the first stage cost, representing the investment cost, remained unchanged, while the second stage cost resulted in a negative value, indicating a profit made from energy arbitrage during the operational phase. The optimization ran for multiple iterations, adjusting decision variables such as energy storage dispatch and generation to ensure convergence. The range of uncertainty, upper and lower bounds, and optimality gap were carefully monitored to determine the stopping criteria.

Table. 5 provides an overview of the bounds and optimality gaps under different confidence levels for the optimization of Type II storage configurations. The table highlights the iterative process of reducing the gap between the lower bound and upper bound until convergence is achieved. For each instance, corresponding to confidence levels ranging from 50% to 95%, the optimization proceeds through three iterations. As the confidence level increases, the total cost also rises, reflecting the higher costs required for robust decision-making under stricter uncertainty requirements. For instance, at a 95% confidence level, the LB and UB values in Iteration 3 are both 7,770,174, achieving convergence with an optimality gap of 0.00%. This

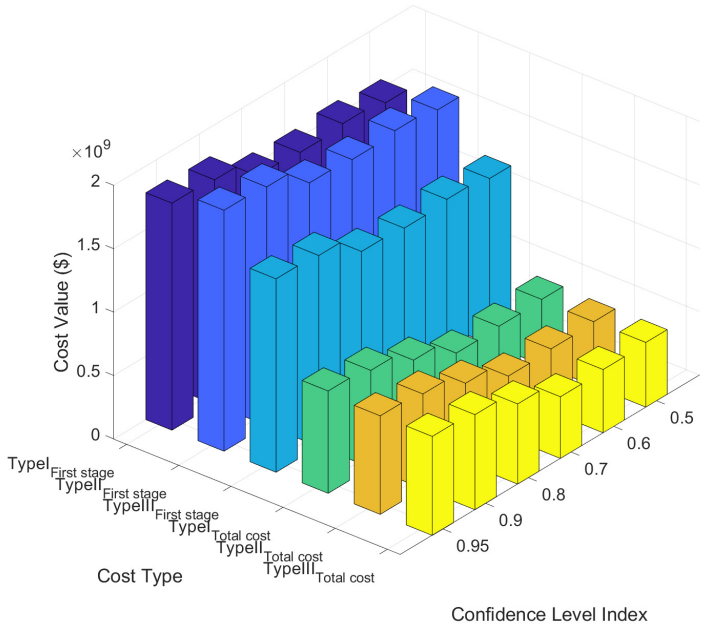

Figure 8: Bar Chart of Different Scenarios Matrix

Table 5: Bounds and gaps under different confidence levels of Type II.

Instance	Confidence level	Iteration	LB	UB	Optimality gap
1	50%	1	-8,265,328	16,380,225	150.46%
	50%	2	4,852,998	5,110,238	5.03 %
	50%	3	5,075,232	5,075,232	0.00%
2	60%	1	-8,265,328	16,325,121	150.63%
	60%	2	4,920,976	4,979,626	1.17%
	60%	3	4,955,382	4,955,382	0.00%
3	70%	1	-8,265,328	16,298,398	150.72%
	70%	2	4,780,853	4,858,691	1.60%
	70%	3	4,835,978	4,835,978	0.00%
4	80%	1	-8,265,328	16,100,244	150.33%
	80%	2	6,236,441	6,305,308	1.09%
	80%	3	6,292,328	6,292,328	0.00%
5	90%	1	-8,265,328	16,879,208	148.97%
	90%	2	7,425,467	7,501,082	1.01%
	90%	3	7,472,174	7,472,174	0.00%
6	95%	1	-8,265,328	16,396,752	150.41%
	95%	2	7,686,453	7,892,186	2.61%
	95%	3	7,770,174	7,770,174	0.00%

trend is consistent across all instances, with convergence achieved within three iterations regardless of the confidence level. The results demonstrate the efficiency and reliability of the optimization process in refining the bounds to achieve optimal solutions under varying uncertainty levels.

5.2.3. Comparison under different Type Energy Storage Systems

It can be observed that at lower confidence levels (0.5, 0.6, 0.7), the storage system output is relatively smooth, with small fluctuations. This is likely because lower confidence levels imply less concern about system uncertainties, resulting in storage being primarily used to smooth load fluctuations and avoid large power changes. On the other hand, at higher confidence levels (0.8, 0.9, 0.95), the variability in storage output increases significantly, especially at the 0.95 level. Fig. 9 to Fig. 11 presents the storage and thermal power outputs under different confidence levels using Type I, which is flywheel energy storage, characterized by a rated power capacity of 7.5 MW and an energy capacity of 1.83 MWh. The storage output shows relatively low variability, with fluctuations around zero, indicating limited reliance on storage to manage uncertainties. The thermal output demonstrates consistent and robust generation, highlighting its role as a resilient energy source under Type I conditions. The minimal impact of varying confidence levels on thermal output underscores its reliability in maintaining system stability.

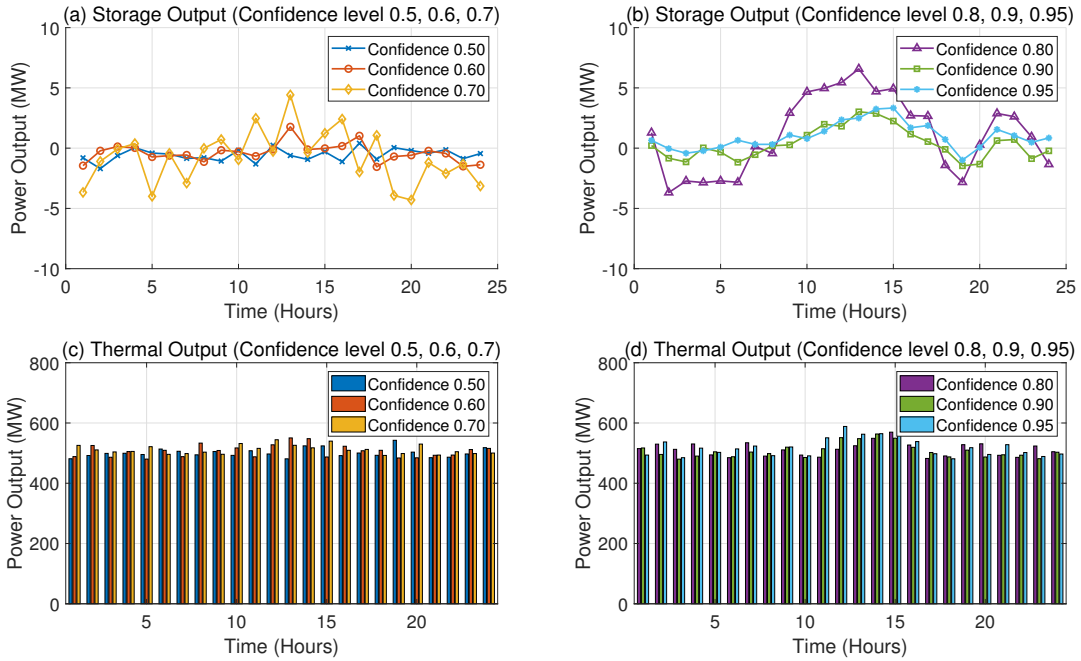

Figure 9: Storage and Thermal Power Outputs with Different Confidence Levels under Type I

From Fig. 9, in Type II, storage output exhibits greater variability, especially during mid-day hours, with higher confidence levels resulting in noticeable peaks. This indicates increased reliance on storage systems to manage uncertainties introduced under Type II conditions, showcasing storage as a flexible but less inherently stable resource. Despite this, the thermal output continues to provide a stable baseline of power, contributing to system resilience by mitigating the impact of storage variability. The slight decrease in thermal output during peak hours suggests the system's adaptive capability to balance storage and thermal contributions effectively.

From Fig. 11, the storage output reaches its highest variability across the three scenarios, especially at higher confidence levels. This highlights storage as a critical but highly dynamic component for maintaining operational resilience under high uncertainty. Peaks in storage output during mid-day emphasize its role in compensating for fluctuations in other parts of the system. Meanwhile, thermal output remains stable and reliable, though minor reductions at lower confidence levels during peak hours suggest some trade-offs between storage and thermal contributions. The comparison across the three figures reveals a progression in system reliance on storage for flexibility and resilience, while thermal generation acts as a consistent backbone, ensuring overall stability. The combination of storage and thermal systems at higher confidence

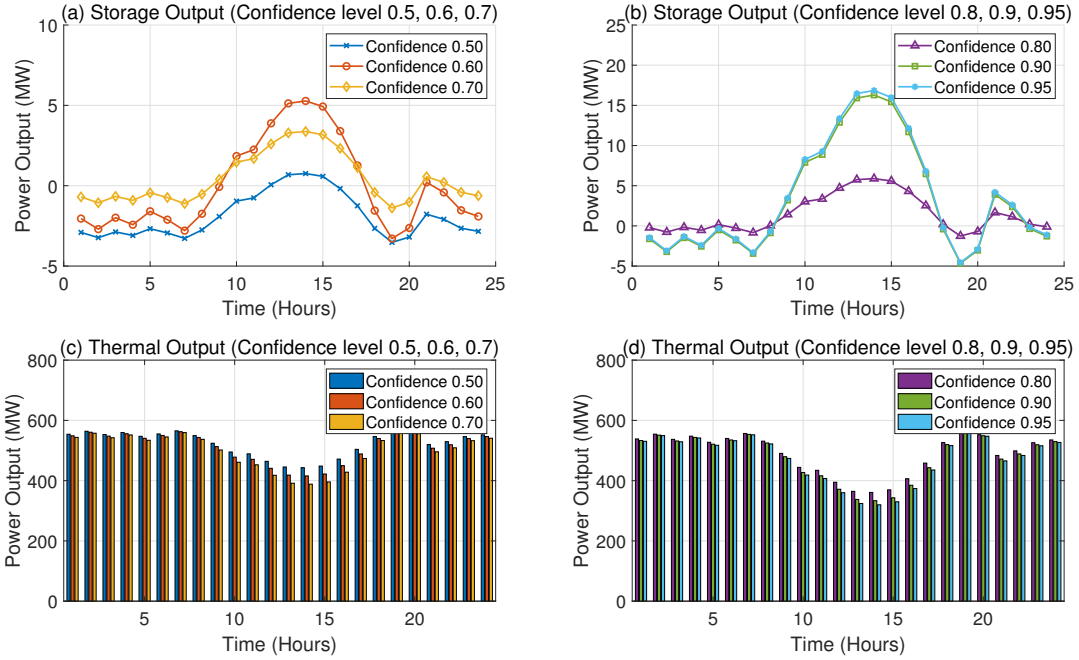

Figure 10: Storage and Thermal Power Outputs with Different Confidence Levels under Type III

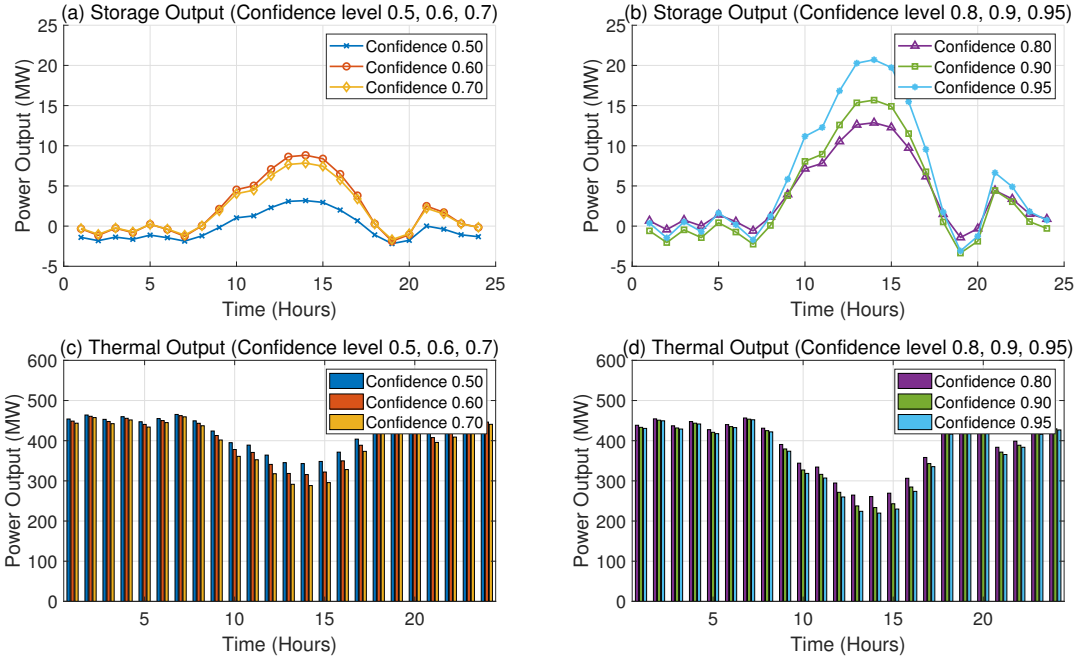

Figure 11: Storage and Thermal Power Outputs with Different Confidence Levels under Type II

levels highlights the trade-off between renewable integration and the need for dependable, conventional generation sources to maintain system stability and reliability.

Fig. 12 compares the frequency deviation suppression performance of different energy storage systems coupled with TPU (Type I, Type II, and Type III) in frequency regulation scenarios. The results demonstrate varying levels of effectiveness in reducing frequency fluctuations across the three types of systems. Under Type I, the TPU-ESS system shows moderate performance in stabilizing frequency. While frequency deviations are reduced compared to the original system, the fluctuations remain relatively prominent. This indicates that Type I ESS has limited capability to fully mitigate frequency instability under these conditions, likely due to lower flexibility or responsiveness in the system design. The Type II ESS achieves the best performance in suppressing frequency deviations among the three systems. The fluctuations are significantly minimized, and the system maintains frequency stability more effectively across the evaluation period.

Table 6: Mean and standard deviation of IQR and range for different ESS types

ESS Type	**Mean IQR (MW)**	**Std of IQR (MW)**	**Mean Range (MW)**	**Std of Range (MW)**
Type I	1.4503	1.7485	2.8248	2.3615
Type II	3.3847	3.4921	6.3093	5.8374
Type III	2.5517	1.7198	6.1411	4.6682

Full statistical sampling is examined for each hour, five representative indicators—minimum, lower quartile, mean, upper quartile, and maximum—are used as proxy points to illustrate the distributional behavior of each ESS type. Fig.13 compares the daily energy storage system output strategies across Type I, Type II, and Type III conditions. In Type I , the output remains close to zero with limited variability throughout the day. The slight fluctuations reflect minor adjustments made by the ESS, indicating relatively stable system conditions and minimal reliance on storage to handle uncertainties. In Type II (subfigure b), the ESS output demonstrates more pronounced variability, particularly during peak hours. This suggests that under Type II conditions, the ESS actively compensates for larger fluctuations in power demand or renewable generation, emphasizing its role in balancing the system. The increased variability highlights the greater challenges in maintaining stability under these conditions. For Type III, the ESS output variability is further amplified, particularly during the mid-day hours. This reflects the ESS taking a critical role in addressing the highest levels of uncertainty and fluctuations under Type III conditions. The broader interquartile ranges in Type III compared to Type I and Type II indicate greater effort by the ESS to maintain system resilience and stability.This setup allows for a comparative assessment of the impacts of both increased capacity and different storage technologies on system variability and performance. To quantify variability, the interquartile range (IQR) and total range (max - min) were computed . Table 6 summarizes the average IQR and range for each ESS type. Both the mean IQR and range increase progressively from Type I to II, confirming the visual assessment of growing variability. Specifically, the mean IQR rises from 1.45 MW in Type I to 3.38 MW in Type II and 2.55 MW in Type III, while the mean total range follows a similar trend. These results illustrate enhanced operational fluctuations with higher-capacity systems and further highlight the effect of storage technology differences, as the the high-capacity flywheel in Type II demonstrates comparable or greater variability than the lithium-ion battery in Type III.

To further evaluate the practical trade-offs among different energy storage configurations, a radar plot analysis is presented in Fig. 14. The results highlight that while the 22.5 MW lithium-ion battery performs well in terms of overall cost-efficiency and moderate electricity loss compared to Type II, but it suffers from higher degradation risks under frequent cycling conditions. In contrast, the 22.5 MW flywheel exhibits superior dynamic performance and virtually no degradation, making it ideal for high-frequency disturbances, albeit at a higher capital cost. The 7.5 MW flywheel shows limited performance due to capacity constraints, but offers a balance between cost and longevity.

6. Conclusion

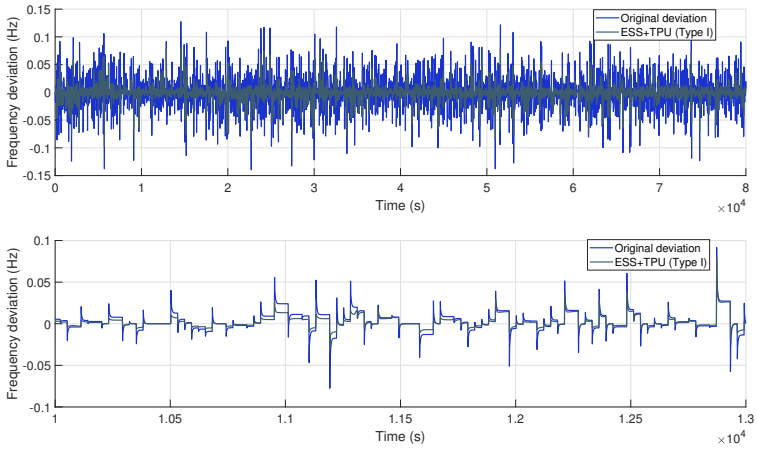

(a) Comparison of Original frequency deviation and TPU-ESS Type I

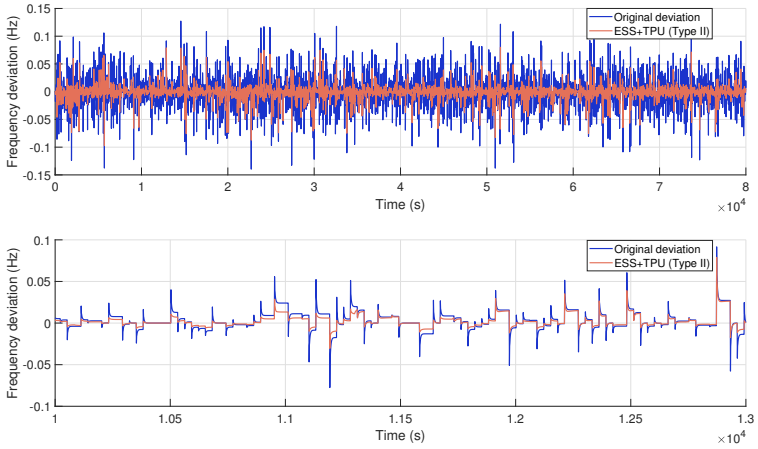

(b) Comparison of Original frequency deviation and TPU-ESS Type I

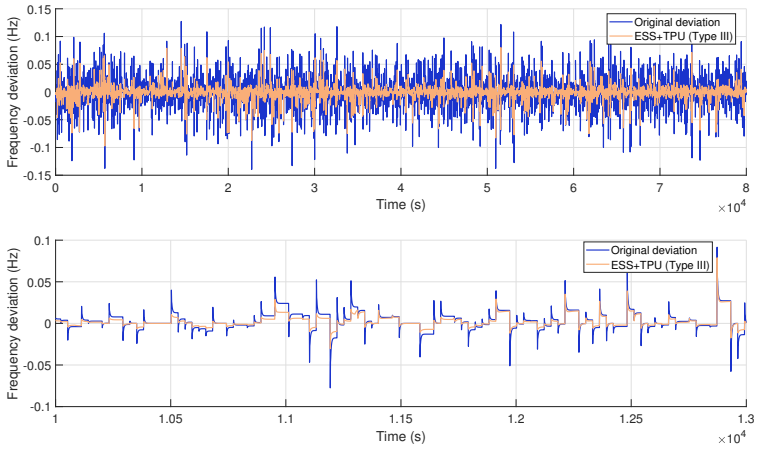

(c) Comparison of Original frequency deviation and TPU-ESS Type I

Figure 12: Storage power output under Type I, Type II, and Type III

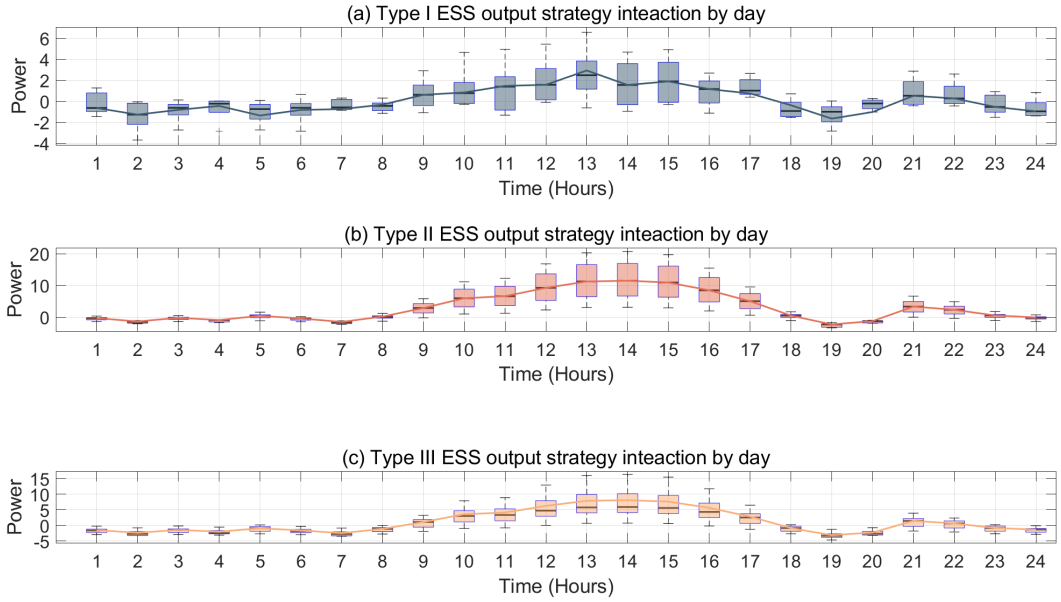

Figure 13: Storage power output under Type I, Type II, and Type III

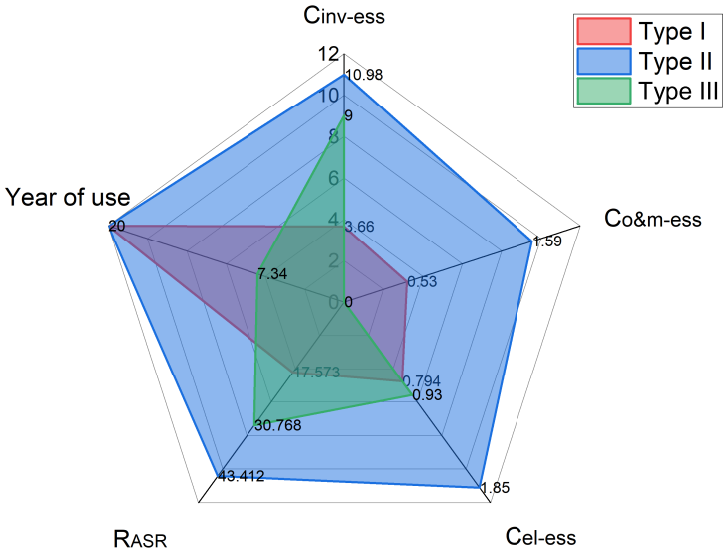

Figure 14: Storage sensitivity analysis under Type I, Type II, and Type III(Million dollars)

With the increasing penetration of renewable energy, thermal power units are facing a greater challenger to provide more flexibility in order to maintain the system stability. Energy storage-assisted thermal power units present a promising solution for countries and regions where thermal generation plants still prevail in their power systems but are facing a greater challenge to accommodate more renewable generations to support low carbon transition. Their future capability of offering multi-timescale frequency regulation supports the integration of more renewable generations. The findings indicate that hybrid energy storage-assisted thermal power systems significantly improve the flexibility and economic viability of thermal power generation, ensuring grid stability in high-renewable energy scenarios. The main conclusions are summarized as follows.

1) The integration of energy storage plays a pivotal role in alleviating the operational stress of thermal power units. By providing multi-timescale frequency regulation, energy storage system effectively balances power fluctuations, reducing the need for frequent ramping and deep cycling of thermal power untis. This prolongs the lifespan of thermal power equipment by minimizing mechanical decay. The coordinated operation of energy storage system and thermal power untis allows for more efficient energy dispatch, optimizing fuel consumption and lowering operational costs.

2) A coordinated control strategies for systems with energy storage system is employed, while high-capacity battery energy storage (Type II, III), the ability to compensate more load during peak periods minimizes the fluctuations for thermal power units to operate at full capacity, enhancing system frequency regulation ability. Energy storage system integration ensures a dynamic response to renewable energy fluctuations, improving grid resilience.

3) A comparative analysis of different energy storage system types highlights their role in optimizing dispatch strategies under varying levels of renewable uncertainty. Larger energy storage systems deliver superior economic benefits by minimizing frequent operations of thermal units, reducing fuel costs, and lowering maintenance expenses. Despite higher initial investments, the cost-benefit analysis reveals that the long-term economic and resilience advantages—including reduced costs, improved adaptability, and enhanced system stability—make these hybrid configurations economically viable.

4) Different storage technologies contribute to improving system flexibility and resilience as their characteristics shows diverse abilities under different timescales. While smaller-capacity energy storage system offers limited benefits but with low maintenance and investment cost, larger-capacity systems enable more sustained power output during peak demand, reducing the reliance on thermal power units and effectively mitigating renewable energy variability. The short-term and long-term energy storage systems show different benefits during the operational duration, as the frequency regulations are more frequent than used to be, short-term energy storage system shows a more comparable profits in both technical and economic aspects.

The future research will focus on the refinement of control strategies to further optimize the economic and operational benefits of storage-assisted thermal power systems. This paper overlooked the voltage profile of ESS, detailed modeling of its reactive power support are critical for a comprehensive stability assessment. Furthermore, high dimensional uncertainty sets and decision variables are required to explore by proposing advanced optimization algorithms. Last but not least developing market mechanisms and policy incentives tailored for storage-assisted thermal power units deployment is another research direction. It is anticipated that new frequency regulation ancillary service markets and electric market mechanisms will accelerate large-scale applications of the technology to integrate energy storages with thermal power units.

Acknowledgements

This project was supported by the National Natural Science Foundation of China (No.52376007).

References

[1] J. Wu, J. Yan, H. Jia, N. Hatziargyriou, N. Djilali, H. Sun, Integrated energy systems, Applied Energy 167 (2016) 155–157. doi:https://doi.org/10.1016/j.apenergy.2016.02.075.
URL https://www.sciencedirect.com/science/article/pii/S0306261916302124

[2] Y. Cheng, R. Azizipanah-Abarghooee, S. Azizi, L. Ding, V. Terzija, Smart frequency control in low inertia energy systems based on frequency response techniques: A review, Applied Energy 279 (2020) 115798. doi:https://doi.org/10.1016/j.apenergy.2020.115798.
URL https://www.sciencedirect.com/science/article/pii/S0306261920312800

[3] S. N. Hussain, A. Ghosh, Evaluating tracking bifacial solar pv based agrivoltaics system across the uk, Solar Energy 284 (2024) 113102. doi:https://doi.org/10.1016/j.solener.2024.113102.
URL https://www.sciencedirect.com/science/article/pii/S0038092X24007977

[4] G. Yin, M. Duan, Pricing the deep peak regulation service of coal-fired power plants to promote renewable energy integration, Applied Energy 321 (2022) 119391. doi:https://doi.org/10.1016/j.apenergy.2022.119391.
URL https://www.sciencedirect.com/science/article/pii/S0306261922007292

[5] F. Hong, Y. Zhao, W. Ji, J. Hao, F. Fang, J. Liu, A dynamic migration route planning optimization strategy based on real-time energy state observation considering flexibility and energy efficiency of thermal power unit, Applied Energy 377 (2025) 124575. doi:https://doi.org/10.1016/j.apenergy.2024.124575.
URL https://www.sciencedirect.com/science/article/pii/S0306261924019585

[6] W. Ji, F. Hong, Y. Zhao, L. Liang, J. Hao, F. Fang, J. Liu, A real-time phase transition modeling of supercritical steam cycle and load variation rate enhancement of thermal power plants under deep peak shaving, Energy 312 (2024) 133431. doi:https://doi.org/10.1016/j.energy.2024.133431.
URL https://www.sciencedirect.com/science/article/pii/S0360544224032079

[7] F. Hong, W. Ji, Y. Pang, J. Hao, M. Du, F. Fang, J. Liu, A new energy state-based modeling and performance assessment method for primary frequency control of thermal power plants, Energy 276 (2023) 127594. doi:https://doi.org/10.1016/j.energy.2023.127594.
URL https://www.sciencedirect.com/science/article/pii/S036054422300988X

[8] Zhongguancun Energy Storage Industry Technology Alliance, Energy Storage Industry White Paper 2024, available online: https://www.cnesa.org/information/detail/?column$_i d = 1 id = 6296[Accessed : 2024 - 04 - 10](2024).

[9] H. Yang, Q. Chen, Y. Liu, Y. Ma, D. Zhang, Demand response strategy of user-side energy storage system and its application to reliability improvement, Journal of Energy Storage 92 (2024) 112150. doi:https://doi.org/10.1016/j.est.2024.112150.
URL https://www.sciencedirect.com/science/article/pii/S2352152X24017365

[10] Y. Ding, Q. Xu, L. Hao, Y. Xia, A stackelberg game-based robust optimization for user-side energy storage configuration and power pricing, Energy 283 (2023) 128429. doi:https://doi.org/10.1016/j.energy.2023.128429.
URL https://www.sciencedirect.com/science/article/pii/S0360544223018236

[11] J. Cui, Z. Zhu, G. Qu, Y. Wang, R. Li, Demand-side shared energy storage pricing strategy based on stackelberg-nash game, International Journal of Electrical Power Energy Systems 164 (2025) 110387. doi:https://doi.org/10.1016/j.ijepes.2024.110387.
URL https://www.sciencedirect.com/science/article/pii/S0142061524006100

[12] J. Zhang, J. Wang, N. Zhang, P. Wang, Y. Wang, C. Fang, Droop coefficient placements for grid-side energy storage considering nodal frequency constraints under large disturbances, Applied Energy 357 (2024) 122444. doi:https://doi.org/10.1016/j.apenergy.2023.122444.
URL https://www.sciencedirect.com/science/article/pii/S0306261923018081

[13] C. Li, Y. Cao, B. Li, S. Wang, P. Chen, A novel power control scheme for distributed dfig based on cooperation of hybrid energy storage system and grid-side converter, International Journal of Electrical Power Energy Systems 157 (2024) 109801. doi:https://doi.org/10.1016/j.ijepes.2024.109801.
URL https://www.sciencedirect.com/science/article/pii/S014206152400022X

[14] Y. sheng Xie, Yu-Lee, X. qiang Chang, X. Yin, H. Zheng, Research on the transaction mode and mechanism of grid-side shared energy storage market based on blockchain, Energy Reports 8 (2022) 224–229, 2021 6th International Conference on Clean Energy and Power Generation Technology. doi:https://doi.org/10.1016/j.egyr.2021.11.044.
URL https://www.sciencedirect.com/science/article/pii/S2352484721011896

[15] M. Khani, M. Samiei Moghaddam, T. Noori, R. Ebrahimi, Integrated energy management for enhanced grid flexibility: Optimizing renewable resources and energy storage systems across transmission and distribution networks, Heliyon 10 (20) (2024) e39585. doi:https://doi.org/10.1016/j.heliyon.2024.e39585.
URL https://www.sciencedirect.com/science/article/pii/S2405844024156162

[16] M. Jafarian, E. Assareh, A. Ershadi, X. Wang, Optimal integration of efficient energy storage and renewable sources in hybrid energy systems: A novel optimization and dynamic evaluation strategy, Journal of Energy Storage 101 (2024) 113880. doi:https://doi.org/10.1016/j.est.2024.113880.
URL https://www.sciencedirect.com/science/article/pii/S2352152X24034662

[17] H. Wang, X. Zhang, Y. Sun, Q. Li, Preventive primary frequency response control of energy storage systems for a high renewable penetrated power grid, Electric Power Systems Research 238 (2025) 111109. doi:https://doi.org/10.1016/j.epsr.2024.111109.
URL https://www.sciencedirect.com/science/article/pii/S0378779624009945

[18] R. Zhang, X. Ren, Z. Liu, Z. Bie, C. Chen, Distributed cooperative secondary frequency control for power system penetrated with renewable energy sources and energy storage with communication time delays, International Journal of

Electrical Power Energy Systems 164 (2025) 110411. doi:https://doi.org/10.1016/j.ijepes.2024.110411.
URL https://www.sciencedirect.com/science/article/pii/S0142061524006343
[19] W. Liu, Y. Zheng, X. Zhou, Y. Lv, Q. Chen, Enhanced frequency regulation in pumped hydro storage integrated power systems: An innovative modeling method and gpc-pi control strategy, Journal of Energy Storage 103 (2024) 114251. doi:https://doi.org/10.1016/j.est.2024.114251.
URL https://www.sciencedirect.com/science/article/pii/S2352152X24038374
[20] A. Heydari, R. Ebrahimi, M. Ghanbari, Eco-environmental dispatch of power system with high penetration wind farms considering demand/source side uncertainties, Electric Power Systems Research 236 (2024) 110925. doi:https://doi.org/10.1016/j.epsr.2024.110925.
URL https://www.sciencedirect.com/science/article/pii/S0378779624008113
[21] T. N. Rateele, L. Z. Thamae, An optimization approach for the economic dispatch incorporating renewable energy resources into lesotho power sources portfolio, Heliyon 9 (4) (2023) e14748. doi:https://doi.org/10.1016/j.heliyon.2023.e14748.
URL https://www.sciencedirect.com/science/article/pii/S2405844023019552
[22] M. Lu, J. Guan, H. Wu, H. Chen, W. Gu, Y. Wu, C. Ling, L. Zhang, Day-ahead optimal dispatching of multi-source power system, Renewable Energy 183 (2022) 435–446. doi:https://doi.org/10.1016/j.renene.2021.10.093.
URL https://www.sciencedirect.com/science/article/pii/S0960148121015597
[23] Q. Yu, Z. Li, X. Han, P. Ju, M. Shahidehpour, End-to-end learning for stochastic preventive dispatch of renewables-rich power systems in abnormal weather conditions, Renewable Energy 234 (2024) 121107. doi:https://doi.org/10.1016/j.renene.2024.121107.
URL https://www.sciencedirect.com/science/article/pii/S0960148124011753
[24] M. Zare, S. Farhang, M. A. Akbari, R. Azizipanah-Abarghooee, P. Trojovský, Optimizing reserve-constrained economic dispatch: Cheetah optimizer with constraint handling method in static/dynamic/single/multi-area systems, Energy 313 (2024) 133681. doi:https://doi.org/10.1016/j.energy.2024.133681.
URL https://www.sciencedirect.com/science/article/pii/S0360544224034595
[25] N. Li, C. Zhao, L. Chen, Connecting automatic generation control and economic dispatch from an optimization view, IEEE Transactions on Control of Network Systems 3 (3) (2016) 254–264. doi:10.1109/TCNS.2015.2459451.
[26] O. Folorunso, R. Sadiku, Y. Hamam, Dispatchable generation analysis and prediction by using machine learning: A case study of south africa, e-Prime - Advances in Electrical Engineering, Electronics and Energy 9 (2024) 100701. doi:https://doi.org/10.1016/j.prime.2024.100701.
URL https://www.sciencedirect.com/science/article/pii/S277267112400281X
[27] T. H. Nguyen, V. C. Nguyen, D. Q. Bui, P. N. Dao, An efficient min/max robust model predictive control for nonlinear discrete-time systems with dynamic disturbance, Chaos, Solitons Fractals 180 (2024) 114551. doi:https://doi.org/10.1016/j.chaos.2024.114551.
URL https://www.sciencedirect.com/science/article/pii/S0960077924001024
[28] T. L. Nguyen, X. S. Mai, P. N. Dao, A robust distributed model predictive control strategy for leader–follower formation control of multiple perturbed wheeled mobile robotics, European Journal of Control 81 (2025) 101160. doi:https://doi.org/10.1016/j.ejcon.2024.101160.
URL https://www.sciencedirect.com/science/article/pii/S0947358024002206
[29] C. Li, X. Wang, J. Li, X. Zhu, C. Jia, Dual-layer control strategy based on economic characterization of lifetime state and frequency regulation limit partition of hybrid energy storage, Journal of Energy Storage 99 (2024) 113326. doi:https://doi.org/10.1016/j.est.2024.113326.
URL https://www.sciencedirect.com/science/article/pii/S2352152X24029128
[30] D.-Q. Yang, M.-J. Li, T. Ma, J.-W. Ni, Z.-Y. Han, Study on adaptive vsg parameters and soc control strategy for pv-hess primary frequency regulation, Energy 314 (2025) 133909. doi:https://doi.org/10.1016/j.energy.2024.133909.
URL https://www.sciencedirect.com/science/article/pii/S0360544224036879
[31] J. Wang, S. Zhang, J. Huo, Y. Zhou, L. Li, T. Han, Dispatch optimization of thermal power unit flexibility transformation under the deep peak shaving demand based on invasive weed optimization, Journal of Cleaner Production 315 (2021) 128047. doi:https://doi.org/10.1016/j.jclepro.2021.128047.
URL https://www.sciencedirect.com/science/article/pii/S0959652621022654
[32] J. Hui, S. Zhu, X. Zhang, Y. Liu, J. Lin, H. Ding, K. Su, X. Cao, Q. Lyu, Experimental study of deep and flexible load adjustment on pulverized coal combustion preheated by a circulating fluidized bed, Journal of Cleaner Production 418 (2023) 138040. doi:https://doi.org/10.1016/j.jclepro.2023.138040.
URL https://www.sciencedirect.com/science/article/pii/S0959652623021984
[33] W. Ji, F. Hong, Y. Zhao, L. Liang, H. Du, J. Hao, F. Fang, J. Liu, Applications of flywheel energy storage system on load frequency regulation combined with various power generations: A review, Renewable Energy 223 (2024) 119975. doi:https://doi.org/10.1016/j.renene.2024.119975.
URL https://www.sciencedirect.com/science/article/pii/S0960148124000405
[34] J. Guo, W. Deng, J. Zheng, Z. Li, Optimal capacity configuration of hydrogen storage systems connecting the electricity-heat network, in: 2023 IEEE/IAS Industrial and Commercial Power System Asia (ICPS Asia), 2023, pp. 1764–1769. doi:10.1109/ICPSAsia58343.2023.10294997.
[35] P. Su, Y. Zhou, J. Wu, Multi-objective scheduling of a steelmaking plant integrated with renewable energy sources and energy storage systems: Balancing costs, emissions and make-span, Journal of Cleaner Production 428 (2023) 139350. doi:https://doi.org/10.1016/j.jclepro.2023.139350.
URL https://www.sciencedirect.com/science/article/pii/S0959652623035084
[36] D. Yang, G. Xu, B. Yusheng, C. Feixiang, C. Xiaoxia, Z. Sheng, Y. Shiye, Y. Jilei, Bi-level optimal sizing and scheduling

of hybrid thermal power-energy storage system for peak shaving, in: F. Sun, Q. Yang, E. Dahlquist, R. Xiong (Eds.), The Proceedings of the 5th International Conference on Energy Storage and Intelligent Vehicles (ICEIV 2022), Springer Nature Singapore, Singapore, 2023, pp. 250–261.

[37] Y. Sun, M. Ban, H. Liu, W. Bai, H. Jiang, Q. Chen, Coordination of maintenance and flexibility retrofit of coal-fired units in generation scheduling, in: 2022 IEEE/IAS Industrial and Commercial Power System Asia (ICPS Asia), 2022, pp. 732–737. doi:10.1109/ICPSAsia55496.2022.9949657.

[38] Y. Cui, K. Jiang, H. Wei, X. Du, A steam combination extraction thermal energy storage scheme in boiler side for coal-fired power plant flexibility retrofit, Journal of Energy Storage 98 (2024) 113038. doi:https://doi.org/10.1016/j.est.2024.113038.
URL https://www.sciencedirect.com/science/article/pii/S2352152X24026240

[39] A. Azad, H. Shateri, Design and optimization of an entirely hybrid renewable energy system (wt/pv/bw/hs/tes/evpl) to supply electrical and thermal loads with considering uncertainties in generation and consumption, Applied Energy 336 (2023) 120782. doi:https://doi.org/10.1016/j.apenergy.2023.120782.
URL https://www.sciencedirect.com/science/article/pii/S0306261923001460

[40] M. Brandt, J. Woods, P. C. Tabares-Velasco, An analytical method for identifying synergies between behind-the-meter battery and thermal energy storage, Journal of Energy Storage 50 (2022) 104216. doi:https://doi.org/10.1016/j.est.2022.104216.
URL https://www.sciencedirect.com/science/article/pii/S2352152X2200247X

[41] M. Bahloul, M. Daoud, S. K. Khadem, Optimal dispatch of battery energy storage for multi-service provision in a collocated pv power plant considering battery ageing, Energy 293 (2024) 130744. doi:https://doi.org/10.1016/j.energy.2024.130744.
URL https://www.sciencedirect.com/science/article/pii/S0360544224005164

[42] C. Li, C. Feng, J. Li, D. Hu, X. Zhu, Comprehensive frequency regulation control strategy of thermal power generating unit and ess considering flexible load simultaneously participating in agc, Journal of Energy Storage 58 (2023) 106394. doi:https://doi.org/10.1016/j.est.2022.106394.
URL https://www.sciencedirect.com/science/article/pii/S2352152X22023830

[43] G. N. D. de Doile, P. Rotella Junior, L. C. S. Rocha, K. Janda, G. Aquila, R. S. Peruchi, P. P. Balestrassi, Feasibility of hybrid wind and photovoltaic distributed generation and battery energy storage systems under techno-economic regulation, Renewable Energy 195 (2022) 1310–1323. doi:https://doi.org/10.1016/j.renene.2022.06.121.
URL https://www.sciencedirect.com/science/article/pii/S0960148122009612

[44] Y. Zhu, J. Liu, D. Zeng, L. Liang, Y. Xie, R. Li, Y. Hu, Energy management strategy and operation strategy of hybrid energy storage system to improve agc performance of thermal power units, Journal of Energy Storage 102 (2024) 114191. doi:https://doi.org/10.1016/j.est.2024.114191.
URL https://www.sciencedirect.com/science/article/pii/S2352152X24037770

[45] S. Yan, Y. Zhang, W. Yin, B. Li, J. Ye, Y. Wu, Y. Zhang, Flexibility enhancement of renewable-penetrated power systems coordinating energy storage deployment and deep peak regulation of thermal generators, Electric Power Systems Research 231 (2024) 110354. doi:https://doi.org/10.1016/j.epsr.2024.110354.
URL https://www.sciencedirect.com/science/article/pii/S0378779624002426

[46] Y. Wang, H. Dong, K. Ma, H. Wang, J. Zhang, Multi frequency stability optimization of integrated energy systems considering virtual energy storage characteristics of heating networks, Applied Thermal Engineering 257 (2024) 124254. doi:https://doi.org/10.1016/j.applthermaleng.2024.124254.
URL https://www.sciencedirect.com/science/article/pii/S1359431124019227

[47] Y. Zhu, S. Yao, Y. Zhang, M. Cao, Environmental and economic scheduling for wind-pumped storage-thermal integrated energy system based on priority ranking, Electric Power Systems Research 231 (2024) 110353. doi:https://doi.org/10.1016/j.epsr.2024.110353.
URL https://www.sciencedirect.com/science/article/pii/S0378779624002414

[48] R. Qin, Y. Lv, F. Fang, D. Deng, B. Wu, N. Mao, J. Liu, Analysis of the improvement in the regulating capacity of thermal power units equipped with flywheel energy storage and the influence on a regional dispatch system, Applied Thermal Engineering 262 (2025) 125248. doi:https://doi.org/10.1016/j.applthermaleng.2024.125248.
URL https://www.sciencedirect.com/science/article/pii/S1359431124029168